UNIVERSIDADE FEDERAL DO PARANÁ

HUGO SEITI YAMASSAKI

GEOMORFOLOGIA SÍSMICA E EVOLUÇÃO DA ARQUITETURA DEPOSICIONAL DE UM LEQUE SUBMARINO NO CRETÁCEO SUPERIOR DA BACIA DE SANTOS

CURITIBA

2021

UNIVERSIDADE FEDERAL DO PARANÁ

HUGO SEITI YAMASSAKI

GEOMORFOLOGIA SÍSMICA E EVOLUÇÃO DA ARQUITETURA DEPOSICIONAL DE UM LEQUE SUBMARINO NO CRETÁCEO SUPERIOR DA BACIA DE SANTOS

Dissertação apresentada como requisito parcial à obtenção do grau de Mestre em Geologia, no Programa de Pós-Graduação em Geologia, Setor de Ciências da Terra, Universidade Federal do Paraná.

Orientação: Prof. Dr. Fernando Farias Vesely

CURITIBA

2021

Catalogação na Fonte: Sistema de Bibliotecas, UFPR
Biblioteca de Ciência e Tecnologia

Y19g

Yamassaki, Hugo Seiti
Geomorfologia sísmica e evolução da arquitetura deposicional de um leque submarino no cretáceo superior da Bacia de Santos [recurso eletrônico] / Hugo Seiti Yamassaki. – Curitiba, 2021.

Dissertação - Universidade Federal do Paraná, Setor de Ciências da Terra, Programa de Pós-Graduação em Geologia, 2021.

Orientador: Fernando Farias Vesely

1. Geomorfologia – Santos, Bacia de (SP). 2. Topografia submarina. 3. Campos petrolíferos. 4. Prospecção sísmica. I. Universidade Federal do Paraná. II. Vesely, Fernando Farias. III. Título.

CDD: 551.408161

Bibliotecário: Elias Barbosa da Silva CRB-9/1894

TERMO DE APROVAÇÃO

Os membros da Banca Examinadora designada pelo Colegiado do Programa de Pós-Graduação em GEOLOGIA da Universidade Federal do Paraná foram convocados para realizar a arguição da Dissertação de Mestrado de **HUGO SEITI YAMASSAKI** intitulada: **GEOMORFOLOGIA SÍSMICA E EVOLUÇÃO DA ARQUITETURA DEPOSICIONAL DE UM LEQUE SUBMARINO NO CRETÁCEO SUPERIOR DA BACIA DE SANTOS**, sob orientação do Prof. Dr. FERNANDO FARIAS VESELY, que após terem inquirido o aluno e realizada a avaliação do trabalho, são de parecer pela sua APROVAÇÃO no rito de defesa.

A outorga do título de mestre está sujeita à homologação pelo colegiado, ao atendimento de todas as indicações e correções solicitadas pela banca e ao pleno atendimento das demandas regimentais do Programa de Pós-Graduação.

CURITIBA, 30 de Março de 2021.

Assinatura Eletrônica
31/03/2021 09:06:00.0
FERNANDO FARIAS VESELY
Presidente da Banca Examinadora (UNIVERSIDADE FEDERAL DO PARANÁ)

Assinatura Eletrônica
31/03/2021 13:10:49.0
PAULO SERGIO GOMES PAIM
Avaliador Externo (UNIVERSIDADE DO VALE DO RIO DOS SINOS)

Assinatura Eletrônica
31/03/2021 09:23:39.0
GILMAR VITAL BUENO
Avaliador Externo (UNIVERSIDADE FEDERAL FLUMINENSE)

Dedico este trabalho aos meus pais, Mary e Roberto.

AGRADECIMENTOS

Agradeço ao meu orientador e amigo professor Dr. Fernando Farias Vesely pela confiança e apoio que me foi entregue durante a elaboração desta pesquisa. Foi muito edificante trabalhar ao lado de um professor com profundo conhecimento geológico e paixão pelo seu ofício.

Ao Programa de Pós-Graduação em Geologia da Universidade Federal do Paraná pela oportunidade de cursar o mestrado de alto nível e inovador, com um corpo docente de excelência.

Ao Laboratório de Análise de Bacias (LABAP) pelo acolhimento e disponibilidade do espaço físico. Destacando os professores Fernando F. Vesely, Barbara Trzaskos, Carlos C.F. Guedes e Carolina D. Aquino e os meus amigos do laboratório Leonardo, Deise, Thammy, Bruno, Ronaldo, Lara, Aurora, Merolyn, Fábio e Nicole.

À Universidade Federal do Paraná, símbolo da ciência do nosso estado e vanguarda em políticas de acessibilidade, prezando sempre pelo valor da igualdade, emancipação e transformação em uma sociedade mais justa.

À Agência Nacional do Petróleo, Gás Natural e Biocombustíveis (ANP) pela liberação dos dados ao laboratório mediante o Processo UFPR-136867 de 26/09/2018.

À Petrobras pelo financiamento da bolsa de pesquisa através do Termo de Cooperação 2016/00284-7 e pelo fomento da pesquisa científica brasileira.

À dGB Earth Sciences pela disponibilização da licença do softwere ‘OpendTect Pro’ e pela sua competente e atenciosa equipe de suporte técnico.

Aos meus amigos da república da Lindinha, Brita, Jun, Itararé e Maciel, que apesar das dificuldades impostas pela pandemia da Covid-19, foi um tempo de muita fraternidade e contentamento que guardarei na memória.

Aos meus pais, Mary e Roberto e meus irmãos Gustavo, Fábio e Marília, por existirem na minha vida.

Aos cientistas brasileiros pela perseverança e dedicação à pesquisa em tempos assombrados pelo negacionismo e irresponsabilidade social.

RESUMO

A geomorfologia sísmica trouxe um outro ponto de vista aplicado à análise de leques submarinos, possibilitando caracterizar a geometria e a composição de elementos deposicionais e reconstituir erosão, transporte e deposição. No entanto, estudos sobre a geomorfologia dos leques submarinos têm se ocupado principalmente em descrever um relativo curto período do tempo geológico, restringindo a interpretação de mudanças geomorfológicas e da arquitetura deposicional em sistemas individuais mais duradouros. Este trabalho apresenta a evolução geomorfológica e a arquitetura do leque submarino Maricá do Cretáceo Superior, norte da Bacia de Santos, região *offshore* SE Brasil. Utilizando sísmica tridimensional, foram mapeados cinco horizontes: Hz1 – base do leque; Hz2 – leque inferior; Hz3 – leque intermediário; Hz4 – leque superior; Hz5 – topo do leque. Isso possibilitou **i)** o acesso às estruturas e elementos do substrato onde o leque foi depositado, à arquitetura interna do leque, ao padrão de empilhamento dos lobos e à morfologia dos canais; **ii)** a medição do comprimento, da sinuosidade e da declividade de 113 canais contidos no leque; **iii)** a observação das mudanças morfológicas e deposicionais que ocorreram através do completo desenvolvimento do leque submarino. O leque submarino Maricá foi depositado diretamente sobre o Escorregamento Maricá e teve sua geometria influenciada pela rugosidade do topo do escorregamento e por altos estruturais causados pela halocinese. A interação entre a topografia do substrato também ocasionou mudanças morfológicas em elementos deposicionais e afetou a distribuição de areia. Seis lobos foram identificados e organizados em ordem estratigráfica (lobo 1 – l2; lobo 2 – L2; lobo 3 – L3; lobo 4 – L4; lobo 5 – L5; lobo 6- L6), revelando padrões agradacionais, progradacionais e eventos de mudança de lobos, apresentando um registro estratigráfico particular. De modo geral, o comprimento e a sinuosidade dos canais aumentam da base para o topo do leque e os dados classificados por lobos revelam que os canais tendem a ser mais curtos e menos sinuosos em estágios iniciais de migração de lobos e mais longos e mais sinuosos com a agradação/progradação dos lobos. Quatro tipos de morfologia de canal foram identificados (retilíneo, sinuoso, meandrante e tipo-entrelaçado), indicando que diferentes processos sedimentares ocorreram em um mesmo sistema turbidítico. Atributos sísmicos e dados de poços mostram que o leque submarino Maricá é um leque arenoso e a distribuição dos sedimentos mais grossos ocorrem principalmente como depósitos de preenchimento de canal. Além disso, cada morfologia do canal é responsável por gerar diferentes depósitos e empilhamentos de camadas com consideráveis impactos na qualidade de reservatório.

Palavras-chave: Sísmica 3D. Ambiente marinho profundo. Sistema turbidíticos. Morfologia de canal submarine. Qualidade de reservatório.

ABSTRACT

Seismic geomorphology is a powerful tool to access deep-water fans, allowing to characterize the geometry and composition of depositional elements and to reconstruct erosion, transport, and deposition. However, studies on deep-sea fan geomorphology have been applied mainly to describe a relatively short period of the geological time, preventing the interpretation of changes in geomorphology and the resulting depositional architecture of individual long-lived systems. Here we present the geomorphological evolution and architecture of the Maricá deep-sea fan in the Upper Cretaceous, northern Santos Basin, offshore SE Brazil. Using three-dimensional seismic data, we mapped five horizons (stratal slices): Hz1 – fan base; Hz2 – lower fan; Hz3 – middle fan; Hz4 – upper fan; Hz5 – fan top. Allowing us **i)** to access the deep-sea fan substrate topography, fan internal architecture, lobes stacking pattern, and channels morphology, **ii)** to measure channel length, sinuosity, and slope in 113 channels, and **iii)** to observe morphological and depositional changes throughout the full deep-sea fan development. The Maricá deep-sea fan was deposited directly onto the top topography of the Maricá slump and had its geometry also influenced by structural highs caused by halokinesis. The interaction between the depositional processes and the underlying topography also caused morphological changes in depositional elements and affected sand distribution. We identified six lobes and organized them in the stratigraphic order (lobe 1 – L1; lobe 2 – L2; lobe 3 – L3; lobe 4 – L4; lobe 5 – L5; lobe 6 – L6), reviling patterns of aggradational, progradational, and lobe switching events, resulting in a particular stratigraphic record. The overall channel length and sinuosity increase from base to top and data classified by lobes reveals that channels tend to be shorter and less sinuous at the initial phase of lobe switching and increase in length and sinuosity with lobe aggradation/progradation. Four types of channel morphology were identified (straight, sinuous, meandering, and braided-like), showing that different sedimentary processes occur on the same turbidite system. Seismic attributes and well data indicate that the Maricá deep-sea fan is a sand-rich fan and that coarse-grained sediments occur mainly as channel-fill deposits. Also, each channel morphology is responsible for creating different deposits and set of beds with considerable impact on reservoir quality.

Keywords: 3D seismic. Deep-sea environment. Turbidite system. Submarine channel morphology. Reservoir quality.

LISTA DE FIGURAS

LISTA DE TABELA

SUMÁRIO

1. INTRODUÇÃO

O ambiente marinho profundo é responsável por armazenar grande parte do sedimento continental que foi erodido e transportado em direção ao mar. Uma das feições deposicionais mais importantes de acúmulo de sedimentos alóctones são os leques submarinos (Fig. 1). Os leques submarinos são os maiores depósitos clásticos geneticamente relacionados da Terra (Covault, 2011; Deptuck and Sylvester, 2018). Exemplos modernos como os leques do Bengal, Amazonas, Indus, e Mississippi exibem volumes de centenas de milhares (10^5) de km³ (Walker, 1992; Curray et al., 2003).

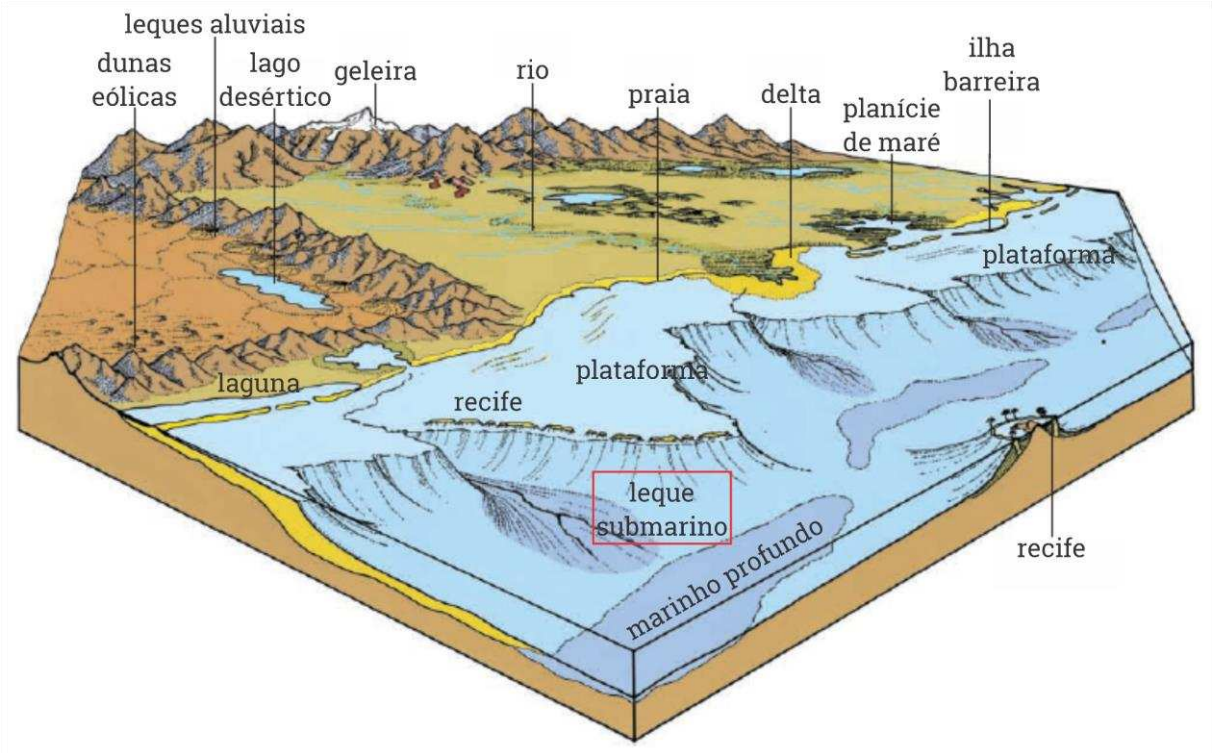

Figura 1 – Bloco diagrama de sistemas deposicionais com destaque para os leques submarinos. Modificado de Hamblin and Christiansen (2003).

Os estudos sobre os leques submarinos possuem grande importância para a indústria do petróleo, pois estas feições deposicionais servem como reservatórios de petróleo e trapas estratigráficas em diversos sistemas petrolíferos e em diferentes estilos de bacias ao redor do mundo (Weimer and Link, 1991; Pettingill and Weimer, 2002). O tema permanece atual, impulsionado pelas recentes descobertas e desenvolvimento de campos de petróleo com reservatórios em arenitos turbidíticos na Bacia da Guiana, *offshore* Guiana, América do Sul Equatorial, estimulados após a descoberta em 2012 do campo de Jubilee em Gana, *offshore* Leste da África (Bryant et al., 2012; Mello et al., 2013). Além disso, os leques submarinos são estudados como

indicadores de mudanças climáticas, variações eustáticas e atividade tectônica, visto que tais alterações ficam registradas nestas feições deposicionais (Carlson et al., 1999; Bouma, 2001; Covault and Graham, 2010; Reece et al., 2011; Clift, 2017).

O conhecimento sobre leques submarinos teve importantes evoluções desde os trabalhos pioneiros de modelos deposicionais e de fácies de leques submarinos (e.g. Normark, 1970; Mutti and Ricci Lucchi, 1978; Walker, 1978) até o século 21 (ver discussão em Shanmugam, 2016). Com base nos novos e melhores dados adquiridos em levantamentos sísmicos 3D foi possível o desenvolvimento da Geomorfologia Sísmica (Posamentier et al., 2007). A Geomorfologia Sísmica é uma ferramenta voltada à "aplicação das técnicas analíticas pertencentes ao estudo do relevo e a análise de superfícies geomorfológicas antigas e soterradas imageadas por dados da sísmica 3D" (Posamentier et al., 2007, p.2, tradução nossa). Esta técnica permitiu um maior detalhamento dos leques submarinos sob o enfoque quantitativo, possibilitando comparações entre elementos deposicionais modernos e antigos de forma mais objetiva. No entanto, a maioria dos trabalhos é focada em estudos da superfície fundo do mar ou subsuperfície rasa, havendo poucos estudos sobre mudanças geomorfológicas e da arquitetura deposicional em sistemas individuais mais duradouros. Dessa forma, o estudo da evolução arquitetônica de sistemas turbidíticos em escalas de tempo mais longas é restrito aos estudos de afloramentos, que carecem da visão em planta obtida pela geomorfologia sísmica.

Neste trabalho realizamos uma análise da evolução geomorfológica de um leque submarino soterrado a ~3100 m abaixo do fundo do mar, no Cretáceo Superior no norte da Bacia de Santos, região *offshore* do sudeste do Brasil. O mapeamento de múltiplos horizontes ao longo de toda sucessão do leque submarino possibilitou **i)** o acesso às estruturas e elementos do substrato onde o leque foi depositado, à arquitetura interna do leque, ao padrão de empilhamento dos lobos e à morfologia dos canais; **ii)** a medição do comprimento, da sinuosidade e da declividade de 113 canais; **iii)** a observação das mudanças morfológicas e deposicionais que ocorreram através do completo desenvolvimento do leque submarino. A pesquisa teve foco na caracterização geomorfológica de elementos deposicionais em diferentes estágios de crescimento do leque submarino e na interpretação da evolução da sua arquitetura deposicional, buscando compreender como os parâmetros comprimento, sinuosidade e declividade dos canais variam em função da evolução do leque submarino, estabelecer correlações entre feições geomorfológicas e registro estratigráfico, utilizar

a geomorfologia como ferramenta para inferir processos sedimentares e apontar possíveis implicações para avaliação da qualidade de reservatórios.

1.1. Área de estudo e contexto geológico

A Bacia de Santos faz parte das bacias marginais da costa leste brasileira, situada na região sudeste, ao longo da costa dos estados do Rio de Janeiro, São Paulo, Paraná e Santa Catarina. A bacia é limitada a nordeste pelo Alto do Cabo Frio, fazendo divisa com a Bacia de Campos, e a sul pela Zona de Fratura de Florianópolis, com fronteira com a Bacia de Pelotas. A área de estudo compreende uma parte do bloco sísmico BS-500, posicionado entre profundidades de 1000 m a 2000 m e a aproximadamente 140 km de distância da costa. A área abrange cinco campos produtivos de petróleo (Tambaú, Uruguá, Tambuatá, Buzios e Itapu) (Fig. 2).

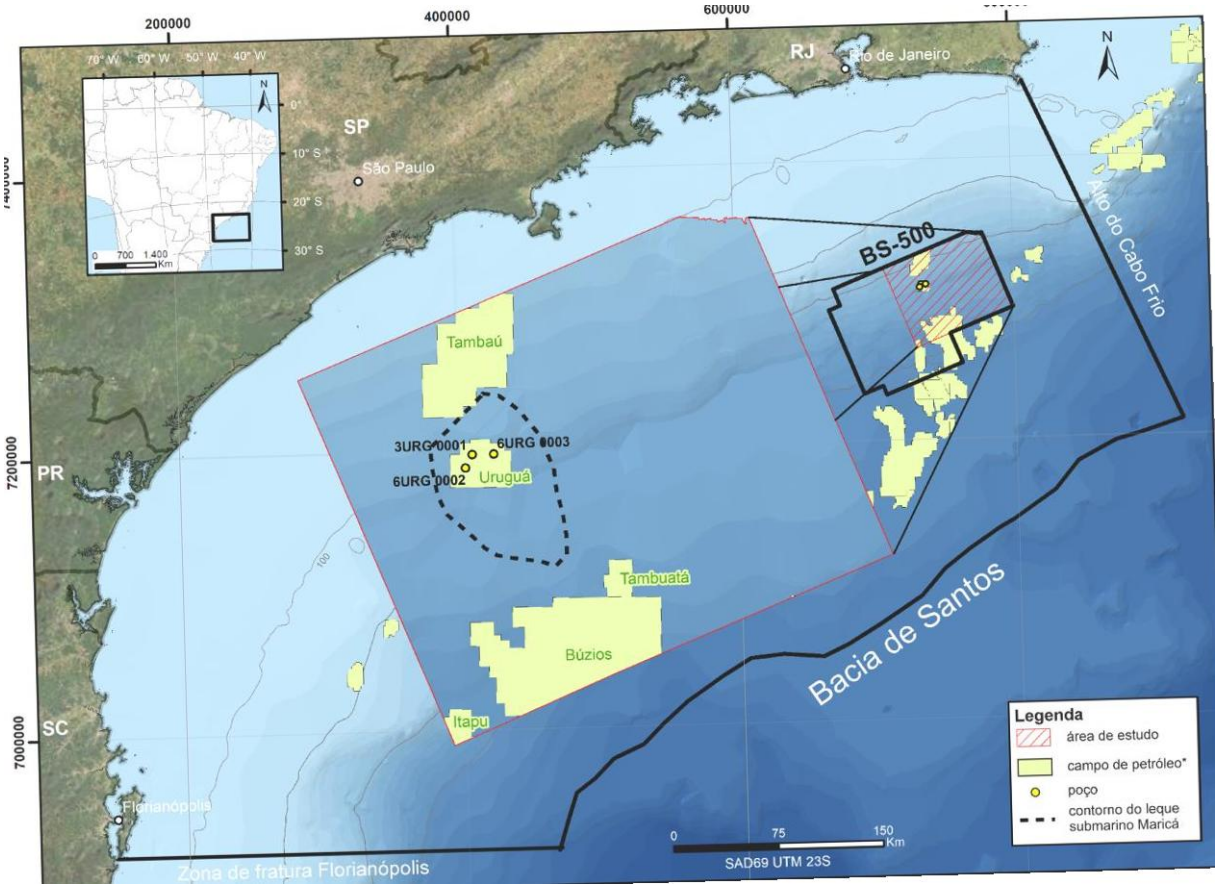

Figura 2 – Mapa da Bacia de Santos e a indicação da área de estudos inserida no levantamento sísmico BS-500. *Fonte ANP (2020).

O início da evolução da Bacia de Santos remete à ruptura do Gondwana, separando o continente Sul-Americano da África durante o Jurássico Superior/Cretáceo Inferior (Mohriak et al., 2008). Moreira et al. (2007) dividem a

história evolutiva da Bacia de Santos em três fases tectônicas: 1ª) fase rifte (Barremiano-Aptiano Inferior); 2ª) fase pós-rifte (Aptiano); 3ª) fase drifte (Albiano-recente). Durante o Aptiano ocorreu a deposição da camada evaporítica responsável pela halocinese que iniciou ainda no Aptiano Superior e teve sua fase de maior atividade durante o Cenomaniano-Maastrichtiano (Quirk et al., 2012). A migração das camadas de sal em direção às porções mais profundas da bacia criou depocentros que foram posteriormente preenchidos por depósitos de sistemas turbidíticos e de fluxos gravitacionais de massa associados à progradação do talude (Assine et al., 2008). Durante o Maastrichtiano a Bacia de Santos registrou a máxima progradação da linha de costa (~200 km) em direção ao oceano durante todo o Cretáceo (Moreira et al., 2007). Esta proeminente progradação foi relacionada ao soerguimento das montanhas da Serra do Mar, ocasionando o incremento do aporte sedimentar para a Bacia de Santos neste período (Modica and Brush, 2004; Zalán and Oliveira, 2005). Também durante o Maastrichtiano, ocorreu a deposição do Escorregamento Maricá, um depósito de transporte de massa (DTM) localizado na base do talude, com um volume de 150 km³ (Carlotto and Rodrigues, 2009). O leque submarino analisado nesta pesquisa foi depositado diretamente sobre o Escorregamento Maricá e por esta razão nós o nomeamos de leque submarino Maricá (Fig. 3).

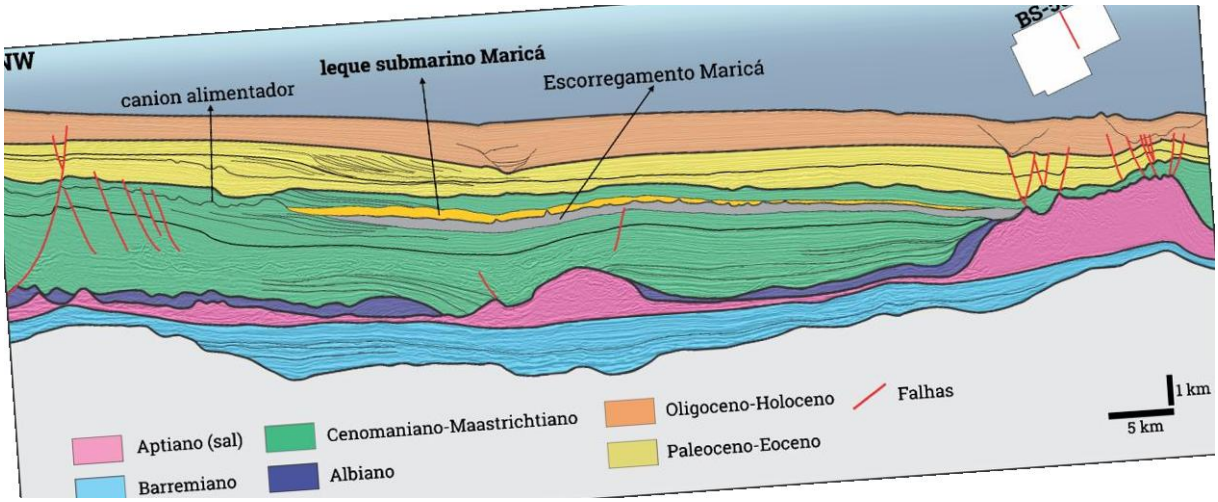

Figura 3 – Seção sísmica dip com a interpretação estratigráfica e o posicionamento do leque submarino Maricá. Baseado em Assine et al. (2008) e Contreras et al. (2010).

2. MATERIAIS E MÉTODOS

O bloco sísmico BS-500 e os dados dos poços foram cedidos pela Agência Nacional de Petróleo, Gás e Biocombustíveis (ANP) ao Laboratório de Análise de

Bacias (LABAP) mediante solicitação formal à instituição (Processo UFPR-136867 de 26/09/2018).

O leque submarino Maricá é completamente coberto pelo levantamento sísmico 3D BS-500, dado sísmico *post-stack* com intervalo de coleta de 2 milissegundos (ms), adquirido em 2000. Os dados sísmicos foram operacionalizados no programa OpendTect Pro 6.4.0. Os poços 6URG 0002, 3URG 0001 e o 6URG 0003 foram utilizados para apoio na análise estratigráfica e para a conversão dos horizontes sísmicos de tempo para profundidade.

Foram mapeados cinco horizontes ao longo do leque submarino, classificados como Hz1 – base do leque (topo do DTM), Hz2 – leque inferior, Hz3 – leque intermediário, Hz4 – leque superior e Hz5 – topo do leque. Cada horizonte representa um determinado tempo de deposição, que combinados formam um *timelapse* da evolução do leque submarino. No Hz1 foi aplicado o atributo sísmico Coerência, com janela de 28, -28 ms, para realçar o talude, as falhas e detalhes morfológicos. Nos horizontes 2 a 5 foi aplicado o atributo sísmico Decomposição Espectral, configurado com a transformada *wavelet* contínua (TWC), *wavelet* gaussiana, com frequência de 41.5 Hz, para salientar a rede de canais, e o atributo sísmico Amplitude Instantânea, para observar as diferenças nas litologias e sua distribuição. O atributo Amplitude Instantânea e Decomposição Espectral foram sobrepostos para gerar as imagens (Apêndice 1).

Foram medidos 113 canais em todo o leque submarino e as medições do comprimento, da sinuosidade e da declividade dos canais foram realizadas no programa ArcGis 10.2.2. A estimativa da sinuosidade dos canais foi medida na escala 1:50.000 e obtida pela razão do comprimento do canal pela distância entre os dois extremos do canal (Fig. 4). O índice de sinuosidade (IS) foi classificado como: retilíneo (IS < 1.1), sinuoso (1.1 <IS> 1.5) e meandrante (IS > 1.5). Para o cálculo da declividade dos canais, primeiramente os horizontes convertidos em profundidade foram horizontalizados a partir de um *datum* em Hz1 – base do leque, para tentar evitar ao máximo o efeito das deformações pós-deposicionais. Em seguida, foi calculado o ΔZ entre as extremidades do canal, dividido o valor obtido pela distância entre as extremidades do canal e o resultado convertido em graus. A tabela de todas as medidas obtidas consta no Apêndice 2.

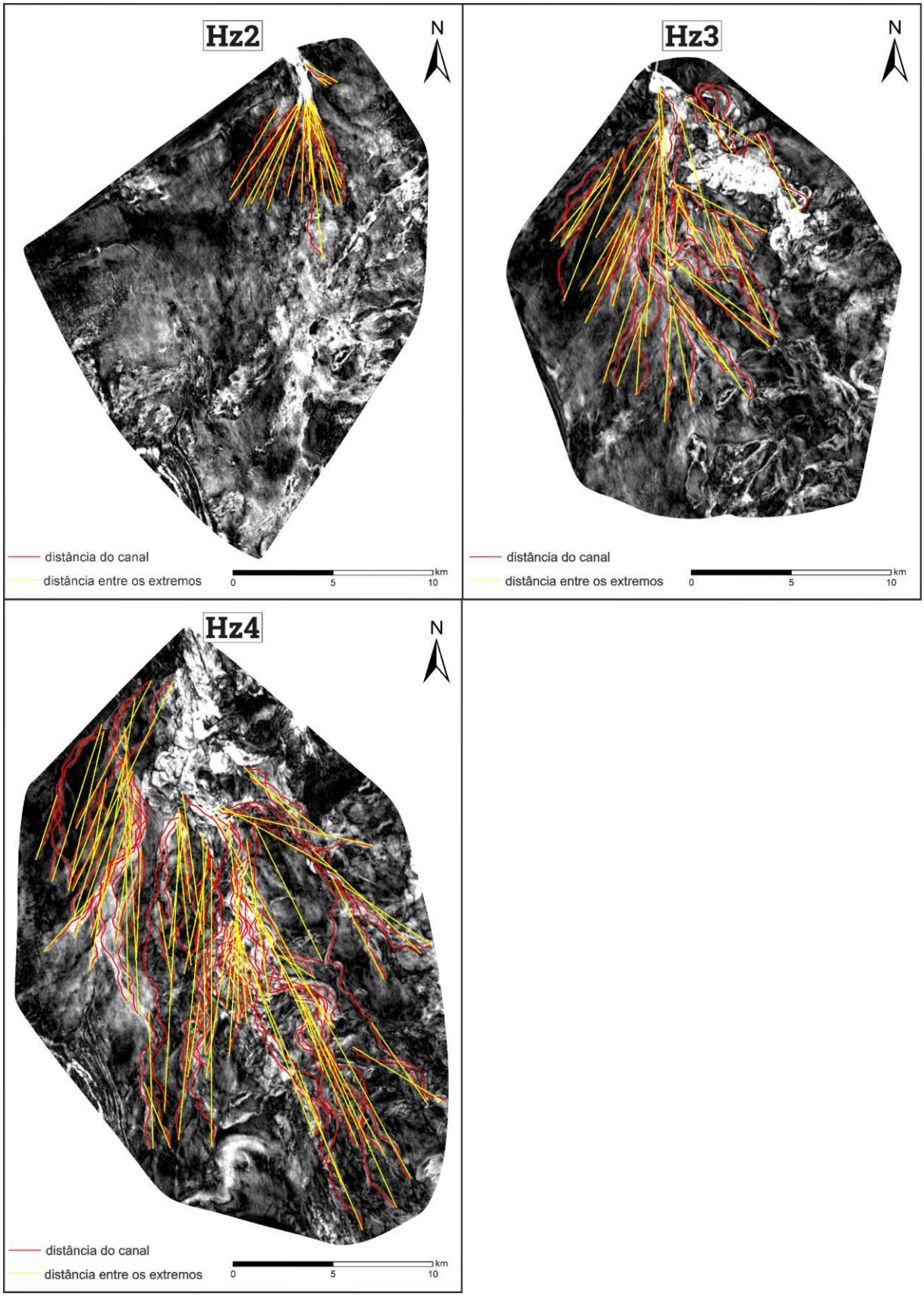

Figura 4 – Método de extração das medidas para o cálculo de comprimento, sinuosidade e declividade dos canais em cada um dos horizontes.

2.1. Terminologia

O conceito de leque submarino utilizado neste trabalho diz respeito a um sistema deposicional representando um lobo composto, alimentado por fluxos gravitacionais de sedimentos através de um cânion encaixado no talude e depositado na bacia, i.e. leque de fundo de bacia (Fisher et al., 2021). O termo ‘lobo’ representa uma feição deposicional formada pelo desconfinamento de correntes turbidíticas e cada lobo é composto por uma rede de canais radiais a partir do seu ápice. O termo ‘espraiamento frontal’ é empregado para pequenos depósitos localizados na porção final de um único canal distributário, formados pelo espraiamento do fluxo devido à diminuição da sua energia. Depósitos de espraiamento frontal não demonstram canais internos observáveis na resolução sísmica disponível.

3. ANÁLISE E DISCUSSÃO DOS RESULTADOS

Os resultados, discussões e conclusões deste trabalho serão apresentados na forma de um artigo científico que será submetido a publicação em uma revista de caráter internacional.

SEISMIC GEOMORPHOLOGY AND DEPOSITIONAL ARCHITECTURE EVOLUTION OF A DEEP-SEA FAN IN THE UPPER CRETACEOUS OF SANTOS BASIN.

Abstract

Seismic geomorphology is a powerful tool to access deep-water fans, allowing to characterize the geometry and composition of depositional elements and to reconstruct erosion, transport, and deposition. However, studies on deep-sea fan geomorphology have been applied mainly to describe a relatively short period of the geological time, preventing the interpretation of changes in geomorphology and the resulting depositional architecture of individual long-lived systems. Here we present the geomorphological evolution and architecture of the Maricá deep-sea fan in the Upper Cretaceous, northern Santos Basin, offshore SE Brazil. Using three-dimensional seismic data, we mapped five horizons (stratal slices): Hz1 – fan base; Hz2 – lower fan; Hz3 – middle fan; Hz4 – upper fan; Hz5 – fan top. Allowing us **i)** to access the deep-sea fan substrate topography, fan internal architecture, lobes stacking pattern, and channels morphology, **ii)** to measure channel length, sinuosity, and slope in 113 channels, and **iii)** to observe morphological and depositional changes throughout the full deep-sea fan development. The Maricá deep-sea fan was deposited directly onto the top topography of the Maricá slump and had its geometry also influenced by structural highs caused by halokinesis. The interaction between the depositional processes and the underlying topography also caused morphological changes in depositional elements and affected sand distribution. We identified six lobes and organized them in the stratigraphic order (lobe 1 – L1; lobe 2 – L2; lobe 3 – L3; lobe 4 – L4; lobe 5 – L5; lobe 6 – L6), reviling patterns of aggradational, progradational, and lobe switching events, resulting in a particular stratigraphic record. The overall channel length and sinuosity increase from base to top and data classified by lobes reveals that channels tend to be shorter and less sinuous at the initial phase of lobe switching and increase in length and sinuosity with lobe aggradation/progradation. Four types of channel morphology were identified (straight, sinuous, meandering, and braided-like), showing that different sedimentary processes occur on the same turbidite system. Seismic attributes and well data indicate that the Maricá deep-sea fan is a sand-rich fan and that coarse-grained sediments occur mainly as channel-fill deposits. Also, each channel morphology is responsible for creating different deposits and set of beds with considerable impact on reservoir quality.

Keywords: 3D seismic; Deep-sea environment; Turbidite system; Submarine channel morphology; Reservoir quality.

4. INTRODUCTION

Deep-sea fans are terminal members of sediment transport from the continent to the deep-sea and are the largest genetically related clastic deposits on Earth (Covault, 2011; Deptuck and Sylvester, 2018). Modern examples like Bengal, Amazon, Indus, and Mississippi fans exhibit volumes of hundreds of thousands km³ (Walker, 1992; Curray et al., 2003). Moreover, deep-sea fans are relevant as reservoirs (turbidite sandstones) of petroleum and stratigraphic traps in many basin settings around the world (Weimer and Link, 1991; Pettingill and Weimer, 2002), with recent major discoveries in the Guyana Basin, offshore Guyana, Equatorial South America, stimulated by the previous discovery of the Jubilee field, offshore Ghana, in the conjugate West African margin (Bryant et al., 2012; Mello et al., 2013). Therefore, deep-sea fans are still promising exploratory targets in frontier basins.

Seismic Geomorphology is a powerful tool to assess deep-water fans, allowing to characterize the geometry, to identify individual depositional elements and reconstruct erosion, transport, and deposition. Previous works show vast applicability of this approach in the study of deep-sea fan morphology and architecture (Hadler-Jacobsen et al., 2005; Covault and Romans, 2009; Babonneau et al., 2012; Jiang et al., 2012; Kolla et al., 2012; Zhang et al., 2018), fan-valley morphology (Kolla et al., 2012), lobes in deep-sea fan (Deptuck et al., 2008; Jegou et al., 2008; Prélat et al., 2010; Picot et al., 2016; Zhang et al., 2016; Doughty-Jones et al., 2017), submarine channels and sedimentary processes (Kolla et al., 2001; Mayall et al., 2006; Wynn et al., 2007, 2012; Janocko et al., 2013; Jobe et al., 2015; Peakall and Sumner, 2015; Reimchen et al., 2016; Lemay et al., 2020), and equilibrium profile and turbidite systems (Pirmez et al., 2000; Ferry et al., 2005; Georgiopoulou and Cartwright, 2013). However, studies of deep-sea fan geomorphology have been applied mainly to describe a relatively short period of the geological time (e.g., surface or near subsurface seafloor), preventing the interpretation of changes in geomorphology and the resulting depositional architecture of individual long-lived systems.

In this study, we examine the geomorphological evolution of a deeply buried (~3100 m below the seafloor) deep-sea fan in the Upper Cretaceous of northern Santos Basin, offshore SE Brazil. By mapping multiple horizons within the fan succession, we were able **i)** to access the deep-sea fan substrate topography, fan internal architecture, lobes stacking pattern, and channels morphology, **ii)** to measure

channel length, sinuosity, and slope in 113 channels; **iii)** to observe morphological and depositional changes throughout the full deep-sea fan development.

4.1. Study area and geological setting

The study area is located in northern Santos Basin, offshore SE Brazil. It lies between the water depths of 1000 m and 2000 m and is 140 km far from the coast (Fig. 5A). This area contains five active producing fields (Tambaú, Uruguá, Tambuatá, Búzios, and Itapu) including reservoirs in both the pre-salt (Aptian) and post-salt (Turonian – Campanian) units, but all taking place stratigraphically below the studied interval.

Moreira et al. (2007) describe three tectonic phases for the evolution history of the Santos Basin: 1st) rift phase (Barremian-Early Aptian); 2nd) post-rift phase (Aptian); 3rd) drift phase (Albian-modern times). The Aptian evaporitic sequence was responsible for an intense halokinesis since the late Albian, with the main phase during the Cenomanian-Maastrichtian interval (Quirk et al., 2012). The salt migration basinward created local depocenters that were later fulfilled with turbidite systems/mass transport deposits associated with shelf progradation (Assine et al., 2008). During the Maastrichtian, the Santos Basin recorded the maximum shoreline progradation (~200 km) of all Cretaceous period (Moreira et al., 2007). This has been related to uplifting in the Serra do Mar coastal range, which increased the sediment supply to the basin (Modica and Brush, 2004; Zalán and Oliveira, 2005). Also in the Maastrichtian, Carlotto and Rodrigues (2009) described the Maricá “slump”, a mass transport deposit (MTD) located at the base of slope to basin floor, with a volume of 150 km³. The deep-sea fan in this study was deposited directly onto the Maricá Slump (Fig. 5B), and for this reason, we named it the Maricá deep-sea fan (MDSF).

5. METHODS

The MDSF is fully covered by the 3D seismic survey BS-500, a post-stack migrated seismic with 2 ms sample interval, acquired in 2000. The wells 6URG 0002, 3URG 0001, and 6URG 0003 were used for stratigraphic analysis and time-depth conversion. We mapped five horizons (stratal slices) related to the deep-sea fan: Hz1 – fan base; Hz2 – lower fan; Hz3 – middle fan; Hz4 – upper fan; Hz5 – fan top. Each one represents a specific depositional time and combined create a timelapse of the

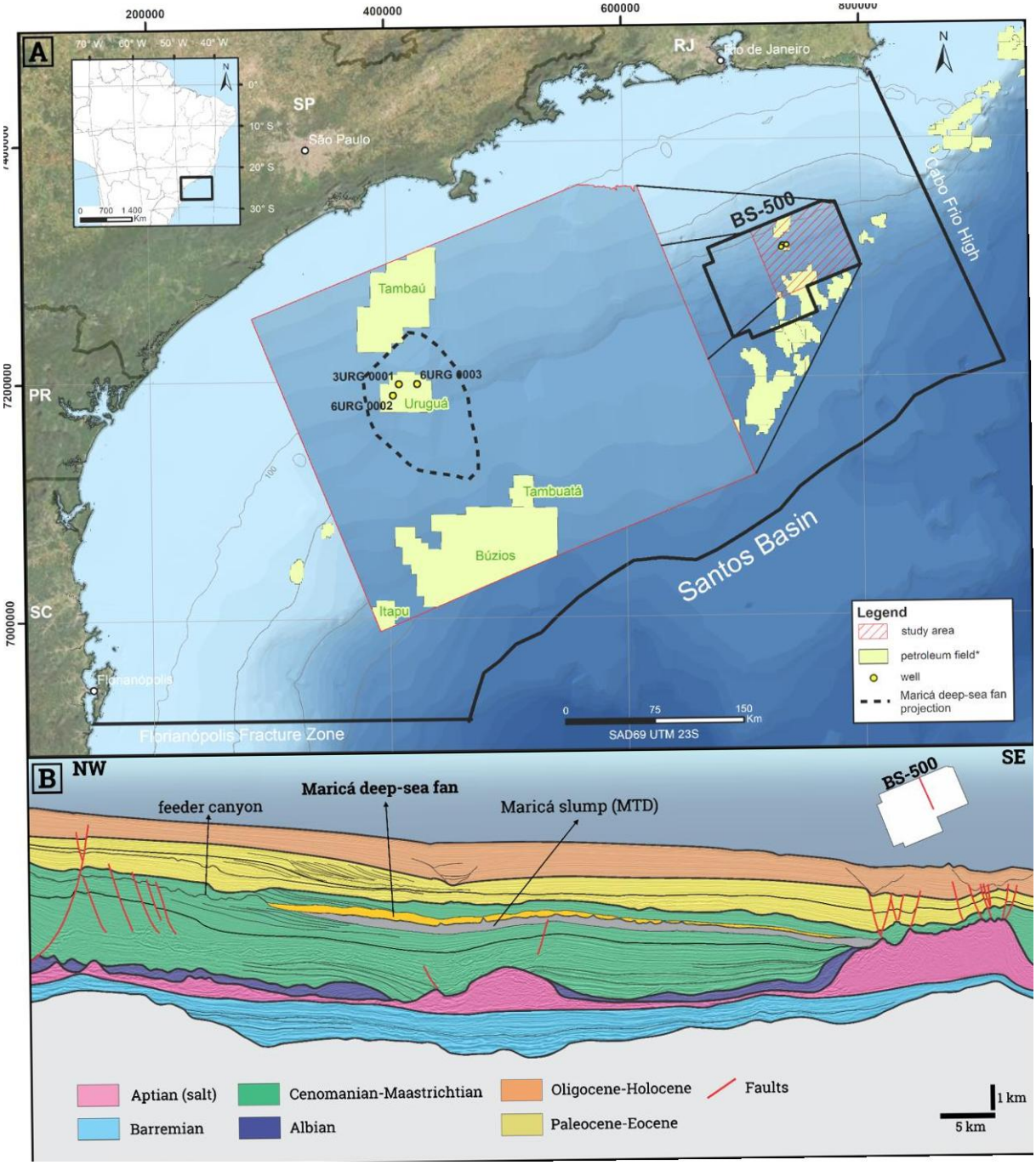

Figure 5 – Location and geological setting. A) Map of the Santos Basin with the study area inside the BS-500 seismic survey (*Source: ANP, 2020). B) Dip-oriented geo-seismic section showing the overall stratigraphy and the MDSF (based on Assine et al., 2008; and Contreras et al., 2010).

deep-sea fan evolution. On Hz1 we applied the Coherence seismic attribute with 28, -28 ms window to highlight the slope, faults, and morphology details. On Hz2-5 we applied the Spectral Decomposition seismic attribute, set up with continuous-wavelet transform (CWT), Gaussian wavelet, and 41.5 Hz output frequency, to illuminate the channel network and the Instantaneous Amplitude seismic attribute to observe differences in lithology and their distribution. We also overlapped the Instantaneous Amplitude and the Spectral Decomposition to generate composite attribute images.

Using the Spectral Decomposition seismic attribute, we estimate the channel sinuosity by measuring the ratio of channel length to the distance between the channel ends in 113 channels (or channel segments) on the entire deep-sea fan, at a 1:50.000 scale. The sinuosity index (SI) was classified as straight (SI < 1.1), sinuous (1.1 < SI > 1.5), and meandering (SI > 1.5). To estimate channel slope, we measured the gradient (ΔZ) along a straight line connecting channel ends on depth-converted horizons referenced to a flattened Hz1. Flattenization was done to reduce at maximum possible post-depositional deformation. We then divided ΔZ by the distance of the channel ends and converted it to degrees.

5.1. Terminology

The examined deep-sea fan is an aggradational, basin floor depositional system composed of multiple lobes and supplied by sediment flows through a shelf-incised canyon (i.e., basin-floor fan; Fisher et al., 2021). We use the term lobe to define a sediment accumulation formed by turbidite flow unconfinement, which is similar to the concept of suprafan lobe (Normark, 1978), fan lobe (Bouma et al., 1985), and lobe (Deptuck et al., 2008). Each lobe is composed of a channel network radiating downflow from its apex. The term frontal (or terminal) splay deposit is employed for smaller deposits, formed at the end of a single distributary channel by flow spreading due to the loss of the flow energy. Frontal splay deposits show no internal channels discernible at the available seismic resolution.

6. RESULTS

6.1. MDSF external morphology and stratigraphic relationships

The MDSF is buried ~3100 m below the seafloor. It has an area of 380 km² and a maximum thickness of 250 m. In dip-oriented sections, fan reflectors onlap the slope face and are downlaped by slope accretion clinoforms (Fig. 6A). The fan thins distally and laterally, and in cross-oriented sections presents a characteristic convex-up top and a flat base (Fig. 6B).

The fan was fed by a shelf-incised canyon with SE paleoflow and developed at the slope-to-basin transition. The isopach map (Fig. 7A) illustrates that the overall fan geometry is elongated at the N-S axis and the depocenter is located close to the

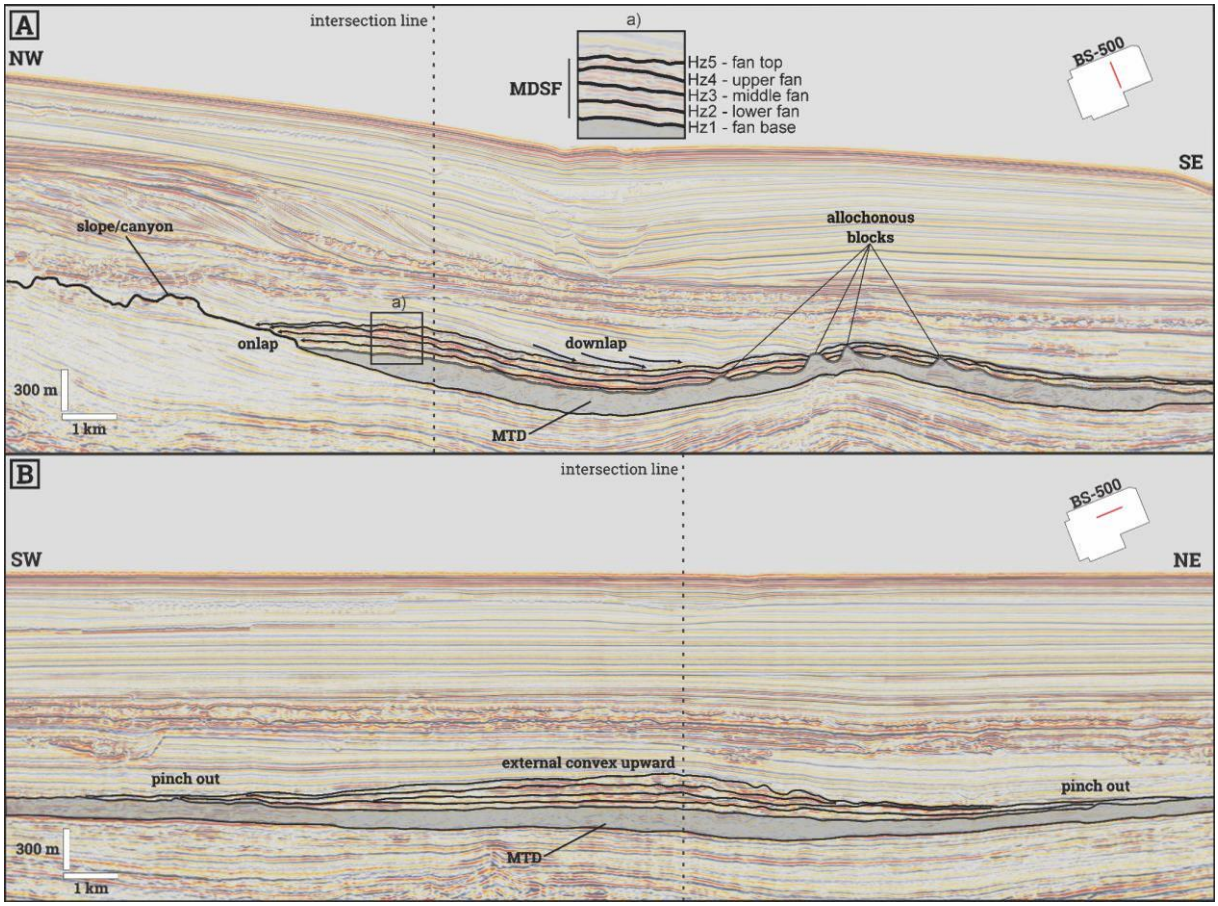

Figure 6 – MDSF external morphology and stratigraphic relationship in A) dip-oriented seismic section with a) indication of five mapped horizons and B) cross-oriented seismic sections.

canyon mouth, but dislocated a little to the southwest whereas the Hz1 structural contour map (Fig. 7B) shows structural highs formed by halokinesis. In section, we can observe fan internal reflectors onlapping on dome surface (Fig. 7C, D), indicating that the MDSF was influenced by an underlying topography controlled by structural highs formed by halokinesis and by the top surface of the Maricá MTD.

6.2. Fan stratigraphy

Within the fan, we identified six lobes (lobe 1 – L1; lobe 2 – L2; lobe 3 – L3; lobe 4 – L4; lobe 5 – L5; lobe 6 – L6) distributed along five mapped horizons and their stratigraphic hierarchy was established based on reflector relationships (Fig. 8), lateral truncation of sets of channels, geographical position, channel morphology, channel sinuosity, and channel density.

Hz1 represents the underlying surface of the MDSF and the top surface of the Maricá slump (MTD) (Fig. 9). It shows the canyon that fed the MDSF, several protrusions related to allochthonous blocks within the MTD (see Fig. 6A) and a dome

rooted by a salt diapir that causes morphological changes on channels and frontal splays.

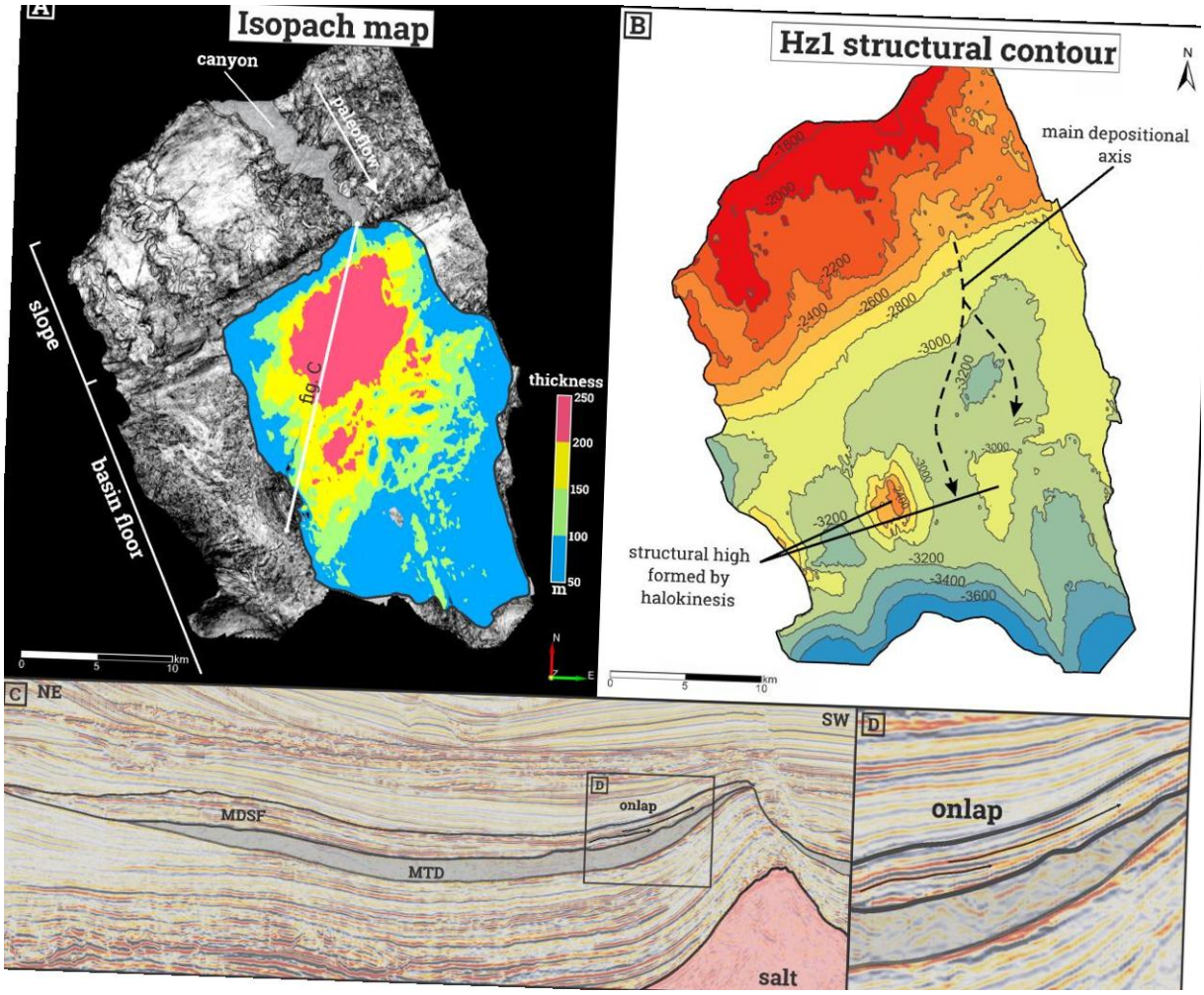

Figure 7 – MDSF external geometry and the influence of the underlying topography. A) Isopach map. B) Hz1 structural contour map showing structural highs rooted by salt domes. C) Dip-oriented seismic section showing fan internal reflectors onlapping on dome surface. D) Detail of onlap reflectors.

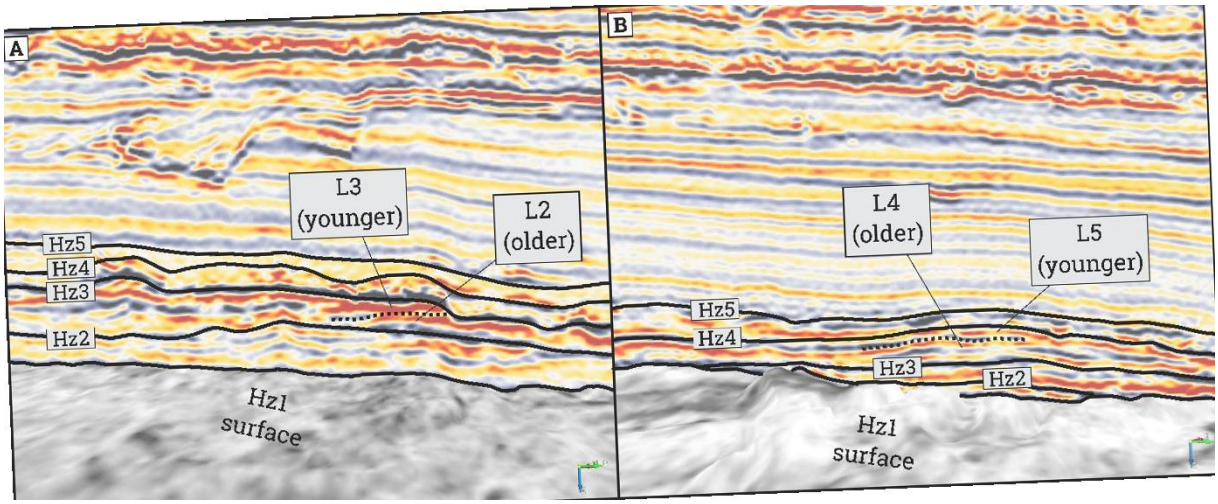

Figure 8 – Lobe stratigraphic hierarchy in cross-oriented seismic sections. A) Stratigraphic relationship between L2 and L3 on Hz3. B) Stratigraphic relationship between L4 and L5 on Hz4.

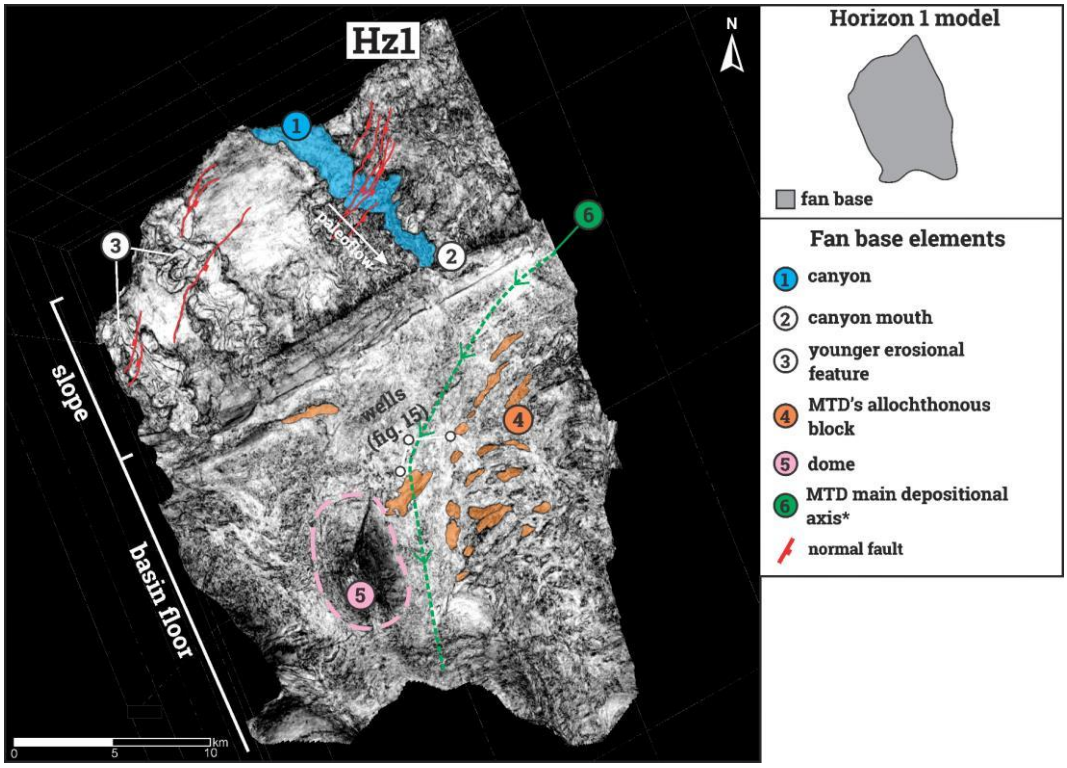

Figure 9 – Interpreted Hz1 map showing the shelf-incised canyon, the allochthonous blocks within the MTD, and the dome rooted by a salt diapir. Seismic attribute: Coherence. *Source: Carlotto and Rodrigues, (2009).

On Hz2, the initial phase of the deep-sea fan growth is represented by a single lobe (L1) with straight channels radiating from the canyon mouth (Fig. 10). At the lobe fringe, we observe a topography constriction caused by the underlying MTD blocks. The development of this lobe is interrupted by an avulsion close to the canyon mouth that consequently forms the L2 observed on Hz3 (Fig. 11). The L2 shows prominent meandering channel belts (only observed in this lobe) that contain most of the sandy deposits of Hz3. The deposition switches to the L3, a progradational lobe whose frontal splays fill the topography caused by the underlying MTD blocks. Also on Hz3, we observe the beginning of the development of the L4. This lobe has more spaced channels with a braided-like morphology. After the deposition of the L2, the input of coarse-grained sediment decrease, being the L3 the lobe with less high amplitude bodies.

On Hz4 we observe the full development of the L4, with wider braided-like channels and sandy frontal splay deposits located next to the base of the dome (Fig. 12). It is followed by L5, representing a strongly progradational lobe with longer sinuous channels. Some of these channels are deflected by underlying MTD topography causing changes in channel course. The L6 developed from an avulsion 7.1 km downstream from the canyon mouth, identified by channel truncation. Sandy deposits

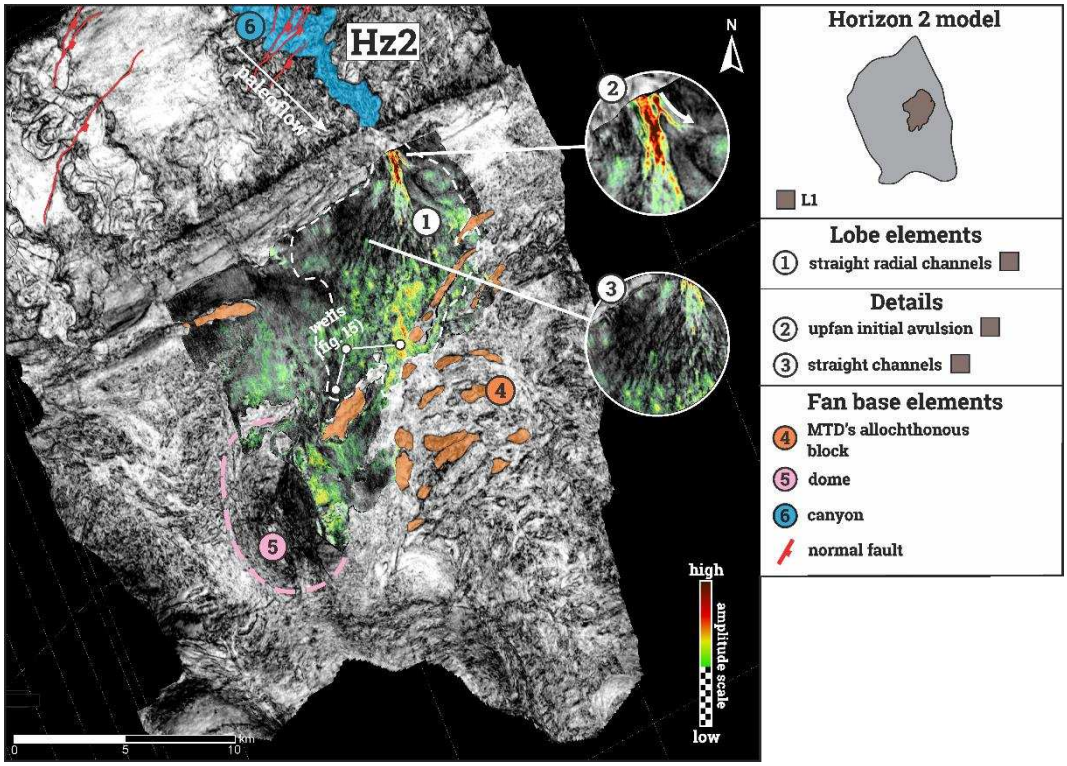

Figure 10 – Interpreted Hz2 with the formation of the L1. Seismic Attribute: Spectral Decomposition and Instantaneous Amplitude.

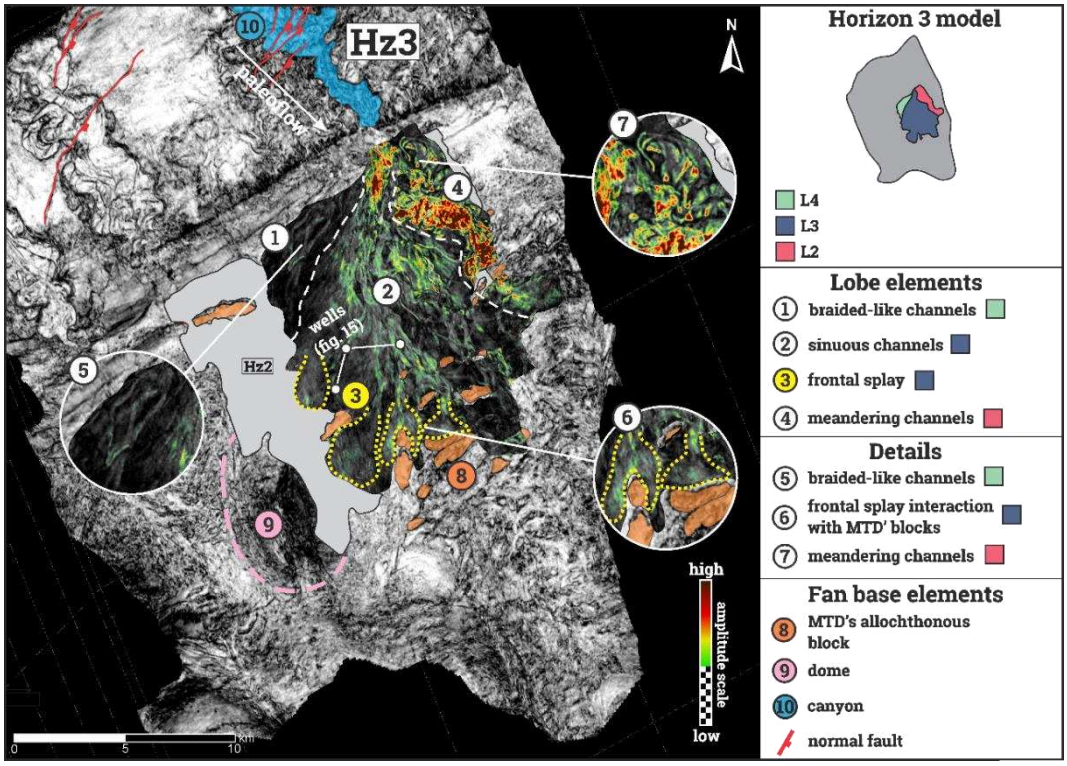

Figure 11 – Interpreted Hz3 with the formation of the L2, L3, and L4. Seismic Attribute: Spectral Decomposition and Instantaneous Amplitude.

are well distributed on Hz4. It occurs on L4 as frontal splays and on L5 and L6 as channel fill deposits. Hz5 shows that the deep-sea fan system became inactive and fully draped by overlying pelagic sediment (Fig. 13).

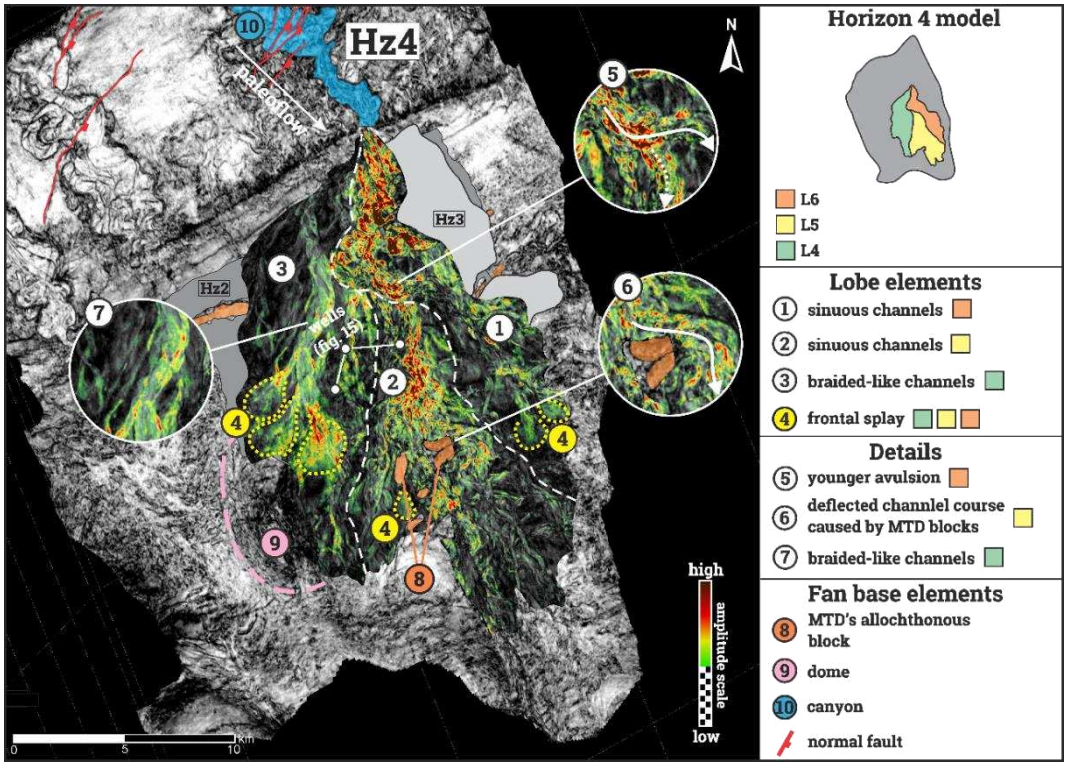

Figure 12 – Interpreted Hz4 with the development of the L4, L5, and L6. Seismic Attribute: Spectral Decomposition and Instantaneous Amplitude.

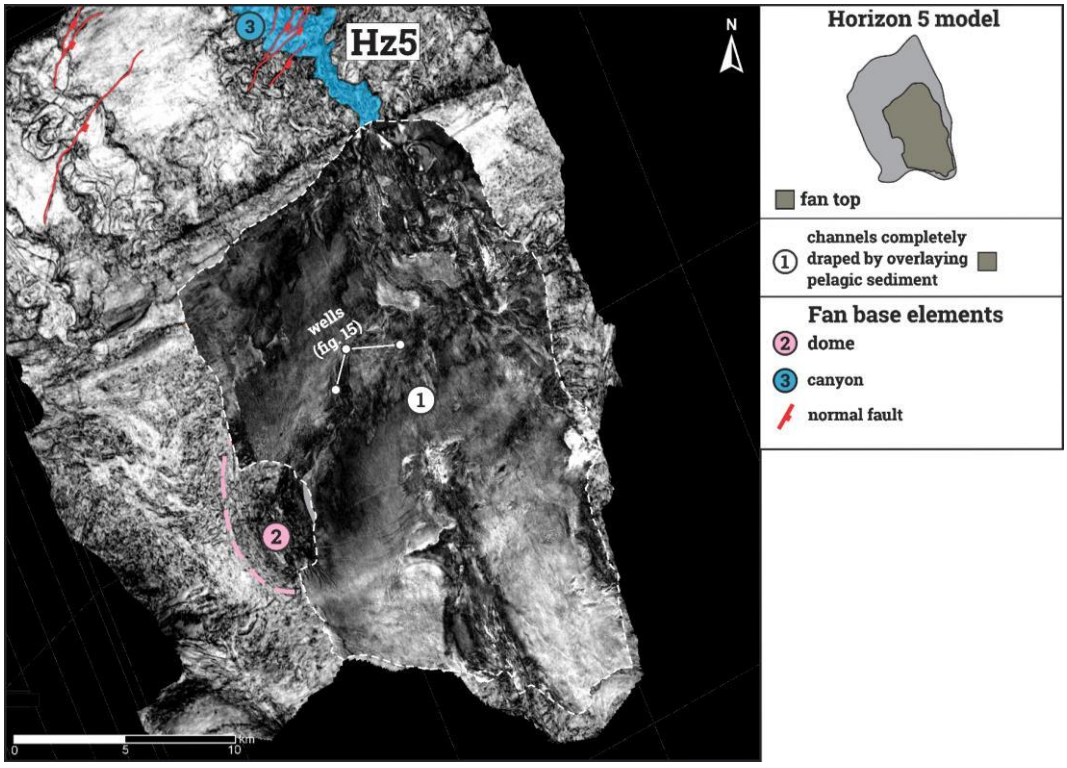

Figure 13 – Interpreted Hz5 showing the end of the Maricá deep-sea fan activity. Seismic Attribute: Spectral Decomposition.

To evaluate the signals of autogenic mechanism on fan internal architecture, we used the previous data on lobes stacking relationship combined with isopach maps of packages in between the examined horizon and the horizon immediately below (Fig.

14). The L1 presents an initial progradational pattern later changing to a more aggradational dominated pattern, showing high thickness values and a relatively small area (Fig. 14A). Hz3 to Hz2 isopach map (Fig. 14B) shows multiple lobe switching cycles marked by local depocenters bounded laterally by relatively thin zones, indicating that at this time the deep-sea fan was strongly dominated by lateral shifts. There is a change when we observe the Hz4 to Hz3 isopach map (Fig. 14C), where lobes present a more pronounced progradational/aggradational pattern. This progradational pattern continues until the end of the fan development (Fig. 14D), with the “possible L4” forming thick deposits between the two structural highs (see Fig. 8B).

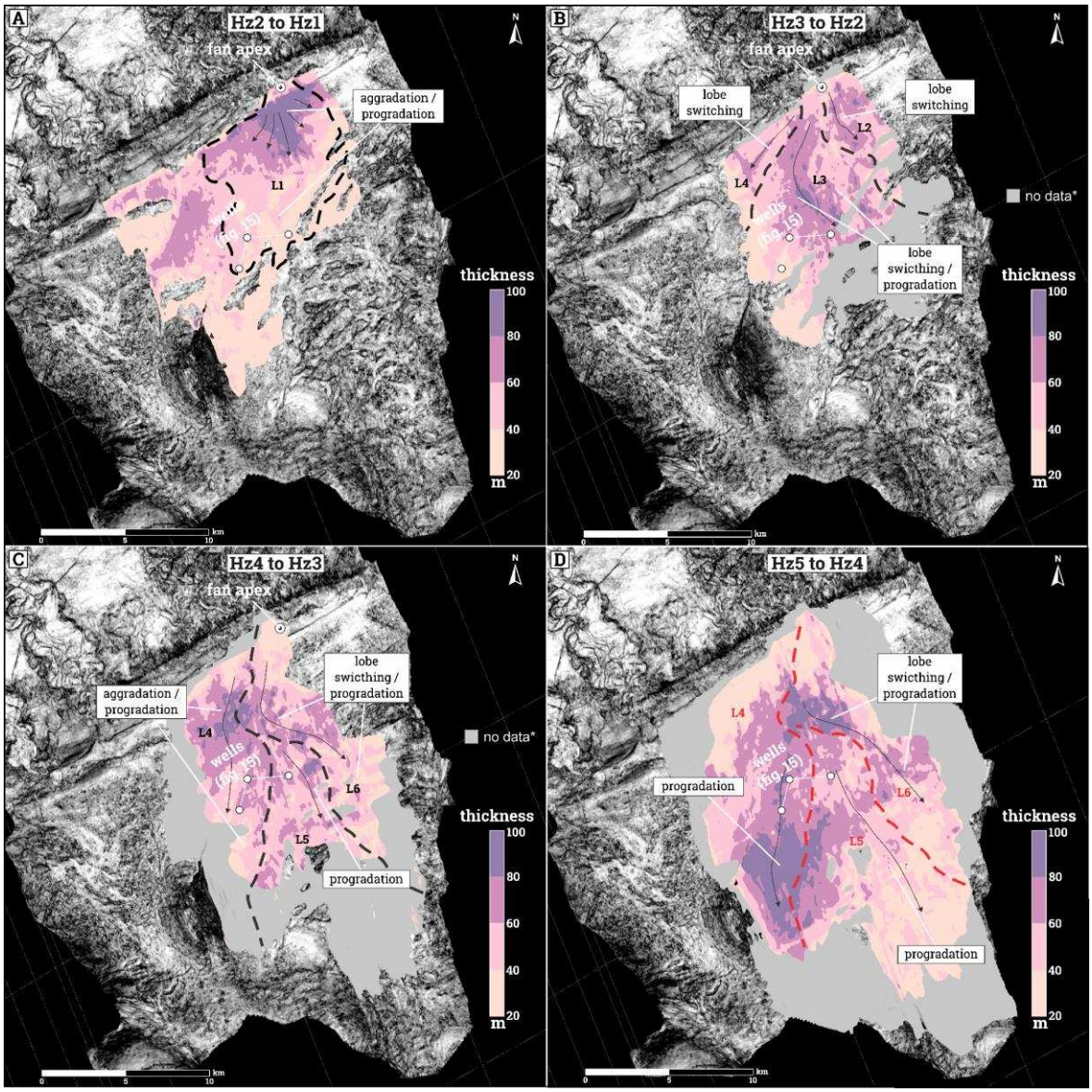

Figure 14 – Lobe aggradation, progradation, and switching cycles. A) Isopach map between Hz2 and Hz1. B) Isopach map between Hz3 and Hz2. C) Isopach map between Hz4 and Hz3. D) Isopach map between Hz5 and Hz4. *Area with no common overlaid surface between horizons. The black dotted line represents interpreted lobe boundary and the red dotted line represents inferred lobe boundary.

The three wells located on the central portion of the MDSF show a Net-to-Gross (N:G) > 70%, indicating a sand-rich fan (Fig. 15). At the base, during the interval between Hz1 and Hz2, the fan records a coarsening-upward pattern caused by the progradation of the initial phase of the fan development. In the middle section, approximately between Hz2 and Hz3, the gamma-ray logs show a fining-upward pattern which is correlated to an interval dominated by fan spreading and lobe switching. Also, the lack of high amplitude regions on L3 suggests higher mud content and corroborates with the gamma-ray pattern. At the top, between Hz3 and Hz5, we observe blocky sandstone successions interbedded with mudstones, which correspond to a phase dominated by fan aggradation and progradation. A lateral change in well-log motifs between Hz4 and Hz5 seems to reflect distinct channel morphologies on different lobes. Wells 6URG 0002 and 3URG 0001 are both located on L4, where braided-like channels take place. This is recorded as thinner sandstone/shale interbeds than in well 6URG 0003 that is located on L5, where sinuous channels are observed (Fig. 12).

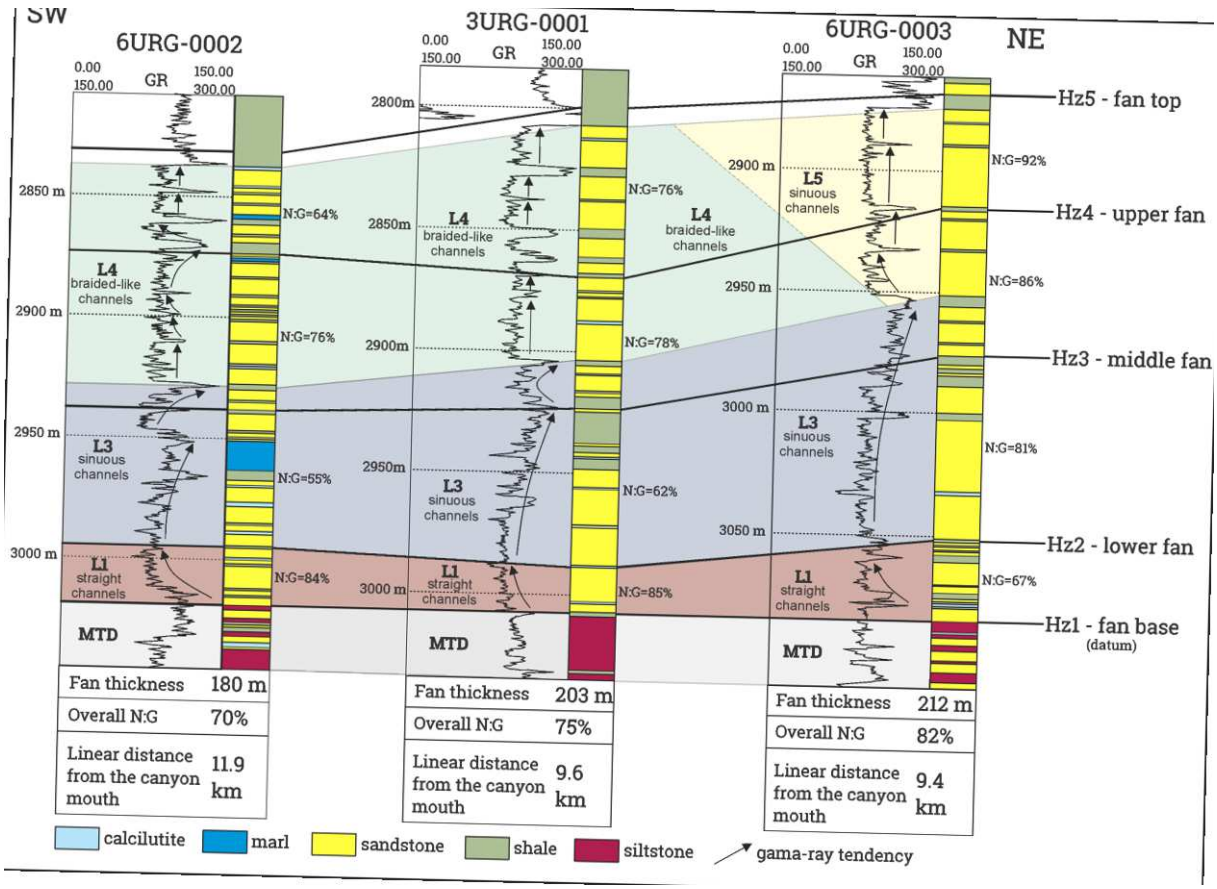

Figure 15 – Well-log correlation with horizons position showing MDSF central portion stratigraphy.

6.3. Channel length, channel sinuosity, and channel slope

From base to top within the fan succession, we observe a general increase in channel length (Fig. 16A) and sinuosity (Fig. 16B), and a decrease in channel slope (Fig. 16C). However, a direct correlation between these parameters is not well determined (low R^2 values), which probably reflects that they are also influenced by other variables such as grain size, flow property, discharge, and lateral compensation (Fig. 16D, E, F).

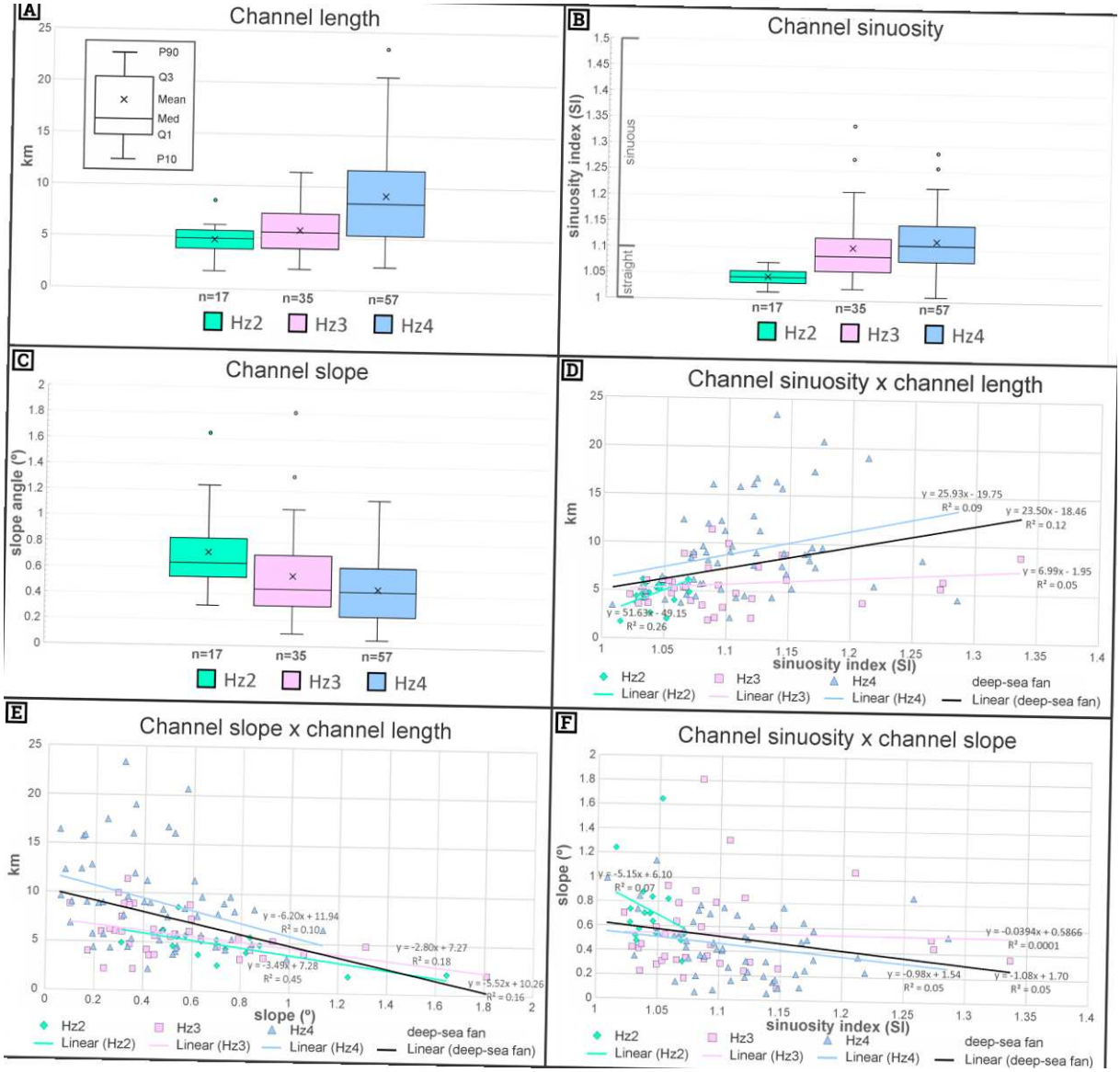

Figure 16 – Channel geomorphologic measurements by horizons (Four out of scale outlier measurements were excluded from this analysis. P90: ninetieth percentile, Q3: third quartile, Med: median, Q1: first quartile, P10: tenth percentile).

To better understand how these parameters vary spatially, we made a detailed plot separated by lobes with an interpreted tendency line (Fig. 17). Data show that the

channel length and sinuosity seem to change as small cycles controlled by lobes development. The tendency line illustrates the interpreted lobes depositional pattern correlated with the channel length plot (Fig. 17A), where channel length increase in periods dominated by lobe aggradation and progradation, and decrease in periods dominated by lobe switching. Similar behavior can be identified in channel sinuosity (Fig. 17B), indicating that channels tend to be less sinuous at the initial phase of lobe switching and increase in sinuosity with lobe aggradation/progradation. However, the channel slope plot (Fig. 17C), besides presenting a slight oscillation during the overall decrease in channel slope, does not show a good correlation with the tendency line. This is probably due to the influence of the underlying topography.

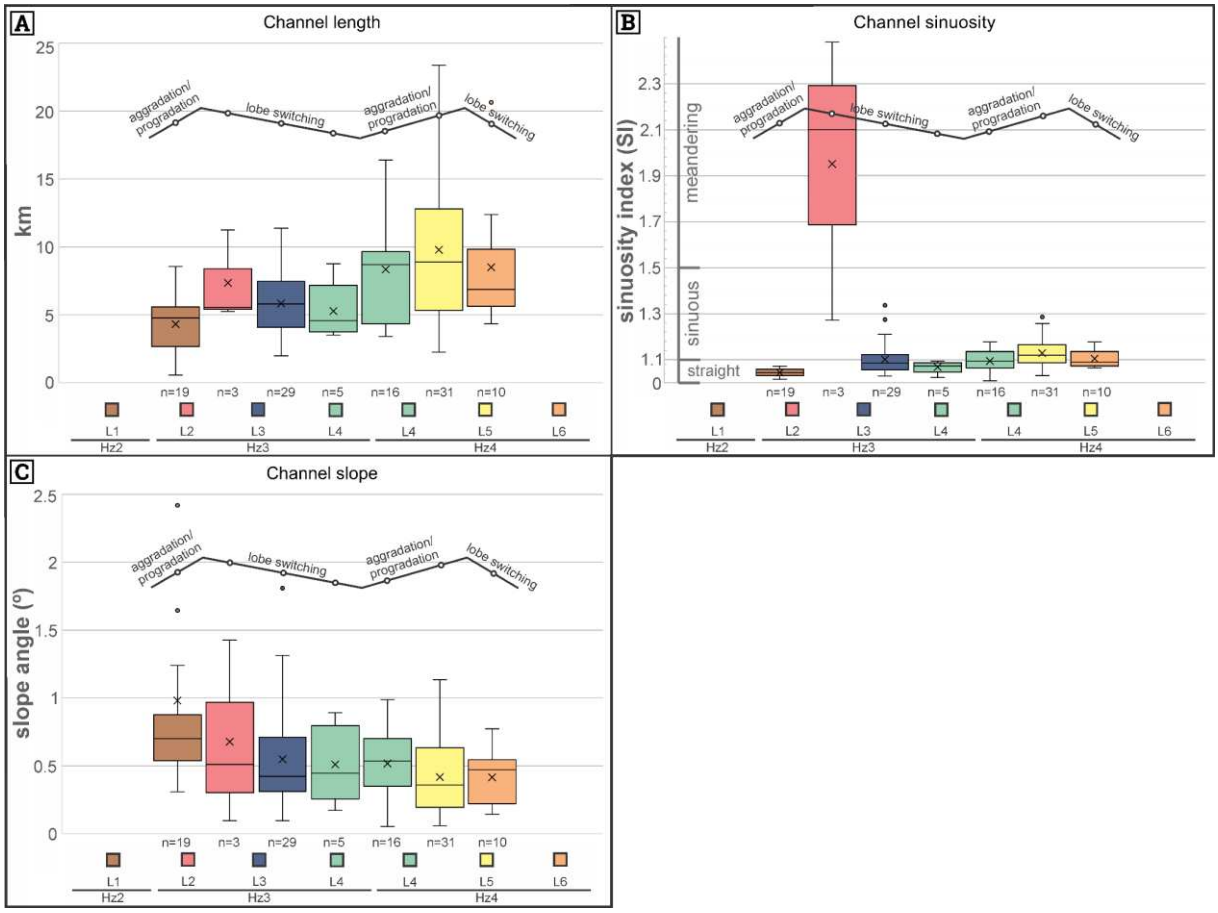

Figure 17 - Channel geomorphologic measurements by lobes with interpreted tendency line.

A synthesis of the data and a resume of channel morphologies, depositional patterns, and sand distribution observed on each lobe can be access in Table 1.

Table 1 – Principal characteristics observed on each lobe.

		channel lenght (mean)	channel sinuosity (mean)	channel slope (mean)	channel morphology	depositional pattern	sandy body occurrences
Hz4	L6	8.5 km	1.10	0.41º	sinuous	lobe switching/ progradation	medium (channel fill)
	L5	9.8 km	1.13	0.42º	sinuous	progradation	high (channel fill)
	L4	8.3 km	1.09	0.52º	braided-like	aggradation/ progradation	medium (fontal splay)
Hz3	L4	5.3 km	1.06	0.51º	braided-like	lobe switching	----
	L3	5.8 km	1.10	0.55º	sinuous	lobe switching/ progradation	low (channel fill)
	L2	7.4 km	1.95	0.68º	meandering	lobe switching	high (channel fill)
Hz2	L1	4.3 km	1.04	0.98º	straight	aggradation/ progradation	low (channel fill)

7. DISCUSSION

7.1. Lobes stacking evolution

A conceptual model of the MDSF evolution is presented (Fig. 18) and illustrates the variability of channel morphology and the stratigraphic stacking of each lobe, forming a composite lobe (Deptuck et al., 2008). The stacking of lobes records a series of events of lobe aggradation, progradation, and switching, presenting a particular interaction with the underlying topography.

After the formation of the L1, the deposition of the L2 occurs in a more confined location than the L3 and the L4, and the further deep-sea fan spreads towards the south and west. Only in the latest depositional event, represented by the L6, lobe migration is towards the east, indicating that the local basin fill started to minimize the influence of basin topography. This process of smoothing local bathymetric relief as the deep-sea fan grows was also described by Covault and Romans (2009). However, this process does not operate equally across the fan. Areas of rapid thickness increase tend to be less and less susceptible to basin topography, whereas areas close to the progradational front may be more susceptible to this topography (e.g., topographically constrained lobe fringe on L1 (Fig. 10) and splay deposits on L3 (Fig 11), and changes in channel course on L5 (Fig. 12).

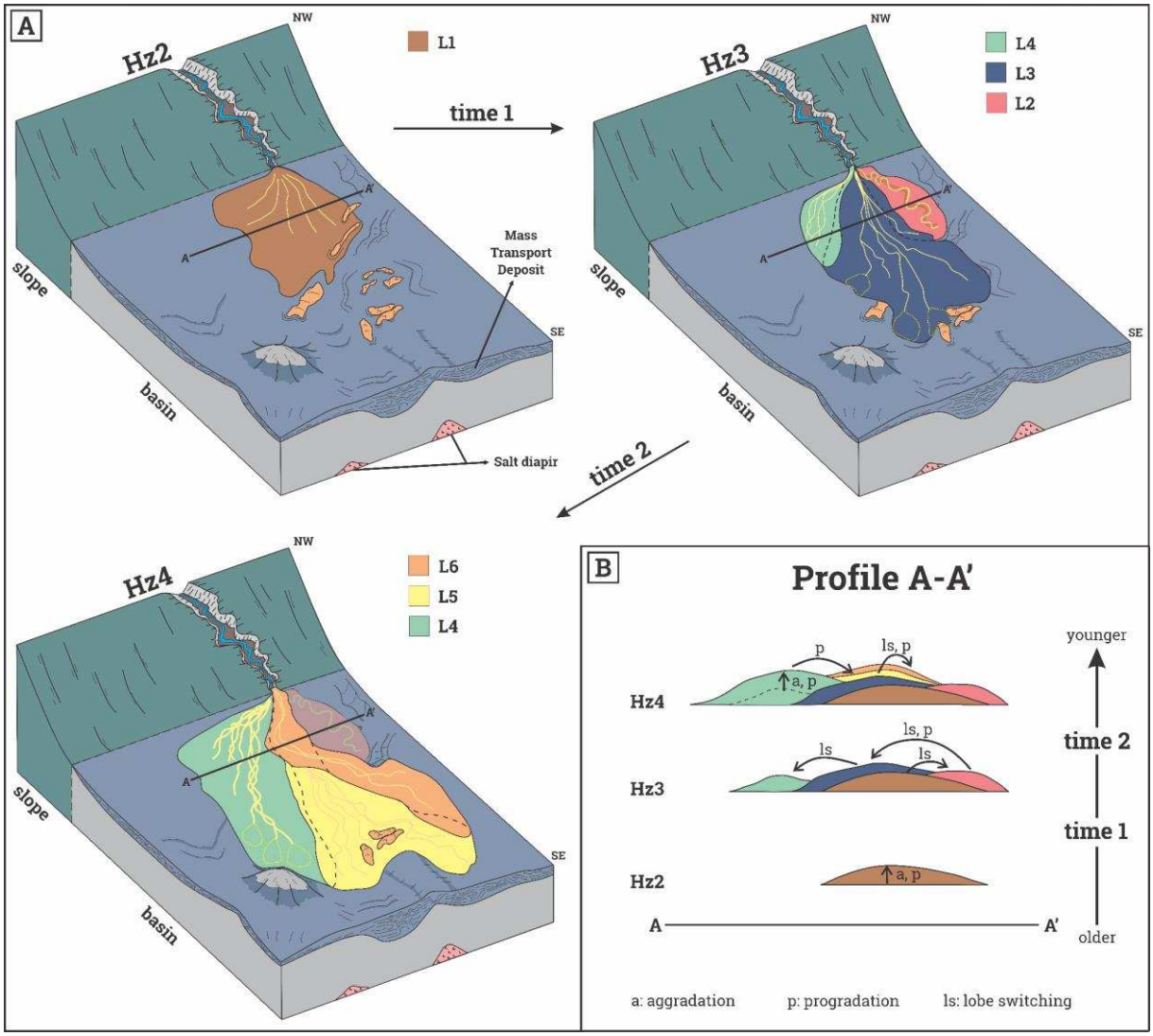

Figure 18 – MDSF depositional model. A) Lobes stacking evolution. B) Profile of the interpreted fan internal architecture.

Another aspect observed is the overall increase in channel sinuosity and the decrease in channel slope (Fig. 16B, C). In terms of slope variation, data from modern alluvial fans show a good correlation between the decrease in the fan slope and the increase in stream discharge (Delorme et al., 2018; Bowman, 2019), leading to a negative correlation between fan area and fan slope (as the fan gets larger, the fan slope decrease). This correlation also occurs in the MDSF, suggesting geomorphological and depositional similarities between subaqueous and subaerial fan-shaped systems. Concerning the inverse relationship between channel sinuosity and slope, Ferry et al. (2005) reported a similar response in a late Miocene system in the Lower Congo basin and interpreted it as a function of the equilibrium profile of the deep-sea fan in a similar way that happen in fluvial landscapes. Our results indicate that this mechanism may operate during deep-sea fan growth, that is, the increase in channel sinuosity as a response to the lowering gradient caused by fan aggradation.

7.2. Controlling factors on channel morphology

Submarine channel morphology is conditioned by multiples factors like flow (velocity, volume, discharge), sediment (volume and grain size), and basin floor (topography and lithology). In addition, despite the submarine channel planform morphology being similar to fluvial channels, they are essentially different in terms of geometry, stratigraphy, flow properties, and depositional dynamics (Kolla et al., 2007; Wynn et al., 2007; Jobe et al., 2016; Lemay et al., 2020). On the entire MDSF four types of channel morphology were identified: straight (Fig. 10), sinuous (Fig. 11, 12), meandering (Fig. 11), and braided-like (Fig. 11, 12). Moreover, different channel morphologies take place in specific lobes and geographical positions, which demonstrates that different sedimentary processes operated on the same turbidite system, but at different times.

Straight channels (SI < 1.1) are dominant on the L1, the first depositional lobe of the deep-sea fan (Fig. 10). By analyzing a submarine channel evolution through time, Gee et al. (2007) and Maier et al. (2013) reported an increase in the channel sinuosity, with straight channels in the early stages. According to these authors, the formation of straight channels would be related to the lack of well-developed levees and weak incisions. Our data propose that straight channels may be formed in the early stages due to the relatively high gradient.

The L2 follows the deposition after the L1 and is the only lobe with meandering channels (SI > 1.5) (Fig. 11). This high and abnormal channel sinuosity can be related to a significant change in flow properties during this time of the deposition. The initial deposition of the L2 happened by an upfan avulsion close to the canyon mouth. Picot et al. (2016) reported that upfan avulsions are less frequent due to higher levees and deeper channels at this portion of the fan and exceptional changes may be necessary to trigger the avulsion, like levee instability and breakup caused by mass movements (Twichell et al., 1996), a local increase in channel sinuosity (Babonneau et al., 2002), discharge of a larger flow volume than usual (Pirmez and Flood, 1995; Kolla, 2007), upfan channel backfill caused by an increase in the sand/mud ratio (Picot et al., 2016). By the time of deposition of the L2, the turbidite flow seems to increase in volume and/or increase the sand/mud ratio triggering the upfan avulsion by overspilling/levee breakup. In this case, the development of the meandering sinuosity could be a

response of channel adjustment for the change in flow conditions to reach equilibrium (i.e., most energy-efficient route; Georgiopoulou and Cartwright, 2013).

Braided channels have been described in modern deep-water environments (e.g., Ercilla et al., 1998; Hesse et al., 2001), but they are much less common than other channel morphologies. Furthermore, sometimes it is not possible to distinguish if the inter-channel braid bars were formed from the instability of the flow-sediment system ('true braiding'), or if they are a result of erosive events, or if they are the irregularity of the sea-floor topography (Wynn et al., 2007; Foreman et al., 2015). Observing the seismic horizon map (Fig. 11, 12), which shows channel overcrossing and high amplitude bodies similar to braid bars, it is not conclusive if the braided channels were formed by 'true braiding'. Foreman et al. (2015) and Limaye et al. (2018) were able to reproduce subaqueous braided channels in flume experiments and reported that braided channels are formed under the condition of a high channel width to depth ratio (> 100). For channels to be able to reach this ratio, the levees build-up must not be high enough to prevent the channel to expand laterally and there must be a non-confined area relative to the volume of the flow. The most developed braided-like channel morphology is observed on the L4 (Fig. 12) and this is the lobe with lesser topographic confinement. Moreover, the sandy frontal splay deposits downstream from these channels could indicate that the flow had high efficiency to carry coarser sediments through the channel, caused by a high velocity rather than a high mud content, which may have contributed to increase channel width and develop a braided-like morphology.

7.3. Implications for sand-body distribution, geometry, and connectivity

The high amplitude zones marked with yellow to dark red colors (Fig. 10, 11, 12) indicate the best potential reservoirs, assuming that they represent the presence of coarser sediments. Also, the well logs (Fig. 15) show that the MDSF has an overall high N:G. In terms of sand distribution, the entire deep-sea fan is strongly dominated by channel-fill deposits, with a few frontal splay deposits. It is secure to expect that majority of the geometry of individual sand bodies are narrow and elongated along the channel axis rather than sheet-like sands with good lateral continuity, implying substantials differences in reservoir properties (see discussion in Bell et al., 2018).

Previous works have described many submarine channel stratigraphy from seismic or/and outcrop data (Kolla et al., 2001; Mayall et al., 2006; McHargue et al., 2011; Gamberi et al., 2013; Janocko et al., 2013; Peakall and Sumner, 2015; Covault et al., 2016). However, analogies should be done carefully because most of them refer to slope channels that are much wider and deeper than these channel networks observed in the MDSF. Bell et al. (2018) describe channel-fill deposits on deep-sea fans as 7 to 9 m successions, thinning- and fining-upward, with basal coarser-grained sandstone with mudclasts overlaid by medium to finer-grained sandstone with traction structures, and upper thin interbedded sandstone and mudstone to stratified mudstone on top. Slump and slide facies originated from the instability of the adjacent channel wall described in slope channels (Mayall et al., 2006; Covault et al., 2016) may be rare in deep-sea fan channels.

The degree on how multiple sand bodies are vertically and laterally connected in the MDSF has a major influence on the reservoir quality. Predictions on this respect can be made by considering the variability of channel morphology and the aggradation/progradation pattern of each lobe. We expect channel bodies to be less vertically connected in lobes with an aggradational pattern, and more laterally connected on lobes with a progradational pattern, and in zones with amalgamated channels. Also, different channel morphologies can form different deposits and architectures. The L2, for instance, has meandering channels that are expected to present laterally extensive bodies as lateral accretion packages (Abreu et al., 2003). For braided channels, Limaye et al. (2018) propose a model that channels tend to migrate laterally at a higher rate than vertically before the channel avulsion, with a tendency to generate deposits with good lateral connectivity. The top portion of well 3URG 0001 presents the stacking pattern of braided-like channels with thinner sandstones/mudstone interbeds than the same interval on the well 6URG 0003, where sinuous and amalgamated channels occur (Fig. 15), showing that, in terms of vertical connectivity, sinuous channels produce better reservoirs than braided-like channels. This is a good example of how to use seismic geomorphology to integrate seismic and well data to shorten the gap resolution between them. In addition, the fining-upward tendency observed on the middle portion of the fan (Fig. 15) can degree the reservoir quality. One explanation for this gradual increase of mud content could be a reduced input of coarser sediments related to clime variation at the source area.

Also, in certain circumstances, the underlying topography may influence deposition, where irregularities can act as obstacles causing instabilities in the flow and major changes in the depositional morphology. Some examples of topographic irregularities are salt domes (Gee and Gawthorpe, 2006; Gamboa et al., 2012; Doughty-Jones et al., 2017; Covault et al., 2019), faults (Georgiopoulou and Cartwright, 2013; Mattos et al., 2019), and mud volcanos (Wood and Mize-Spansky, 2009). In the MDSF, we emphasize two types of underlying topography interaction that affected sand accumulation: the salt dome (which was active during fan development according to Carlotto and Rodrigues, 2009) and the protruding allochthonous blocks of the underlying MTD. The sandy frontal splays on the L4 (Fig. 12) accumulated upslope from the salt dome. We hypothesize that its deposition could be related to the gradual increase in the positive gradient topography towards the dome peak, causing the flow to lose energy and forcing the deposition of coearser sediments. Another possible example happens on the L5 (Fig. 12), where it is visible a concentration of sandy deposits at a distance of ~11,5 km from the fan apex. This sand concentration could be associated with the downstream allochthonous blocks that act as obstacles, which not only caused changes in the channel morphology but also may have generated enough flow instability to deposit coarser sediments upstream.

8. CONCLUSIONS

- With high-quality 3D seismic data, we were able to map five horizons related to the deeply buried MDSF, allowing us to detail the underlying topography, fan architecture, lobes stacking, and channel morphologies.

- The MDSF was fed by a single shelf-incised canyon with the canyon mouth located at the slope-to-basin transition, developing six distinguishable lobes.

- The lobe stacking demonstrates the autogenic accommodation mechanism. The initial stage presents a progradational/aggradational pattern (Hz2), followed by an interval dominated by lobe switching (Hz3) and then changed to an aggradational/progradational pattern (Hz4 and Hz5).

- According to three wells located at the central portion of the fan, the MDSF is a sand-rich fan, with a N:G > 70%. At the base, the coarsing-upward record the progradation of the initial phase of the fan development. The middle portion presents a fining-upward pattern, probably related to the reduced input of coarser sediments at this time. At the top, between Hz3 and Hz5, we observe blocky sandstone successions interbedded with mudstones, which correspond to a phase dominated by fan aggradation and progradation.

- Channel length increase as the fan grows, as well as the channel sinuosity. Conversely, channel slope decreases upward. The channel slope decrease and the channel sinuosity increase upward seems to be a response due to the equilibrium profile as the gradient gets lower with the fan aggradation. The measures classified by lobes reveal that channels tend to be shorter and less sinuous at the initial phase of lobe switching and increase in length and sinuosity with lobe aggradation/progradation.

- We identified four types of channel morphology (straight, sinuous, meandering, and braided-like), and each one takes place in a specific lobe and geographical position, which demonstrates that different sedimentary processes operated on the same turbidite system, but at different times. The variability of channel morphology may be a response to allochthonous changes in the flow properties and the interaction with the local basin topography. Straight channels are common in the early stages of fan growth due to a relatively high gradient. The upfan avulsion that originates the L2 and the high content of sand deposits in this lobe indicates a drastic change in the flow properties that may be responsible for channels to develop the meandering morphology. Braided-like channels seem to be related to a more unconfined topography and a flow with a high velocity and sand/mud ratio.

- Coarse-grained sediments occur mainly as channel-fill deposits, with a few presences of sandy frontal splay deposits. On vertical section, braided-like channel deposits present thinner sandstones/mudstone interbedded compared to sinuous channel deposits.

- We relate a particular interaction with the substrate topography, where sand accumulation is affected by the dome and the underlying MTD blocks.

9. CONSIDERAÇÕES FINAIS

O método de análise geomorfológica por mapeamento de horizontes sísmicos combinado com a estratigrafia sísmica possibilitou acessar as variações morfológicas de um leque submarino soterrado, com um elevado grau de resolução e distribuição tridimensional. É uma poderosa técnica a ser explorada também nos mais diversos ambientes deposicionais, com um vasto potencial ainda a ser descoberto.

O leque submarino Maricá apresenta uma heterogeneidade de morfologias de canais que não é comum quando comparado com outros leques submarinos da literatura, o que nos leva a questionar a eficácia de modelos mais generalistas na predição de distribuição de fácies e caracterizações de reservatórios. Devido a alguns leque submarinos serem bastante sensíveis à topografia da bacia e às variações das propriedades dos fluxos turbidíticos, como é o caso do leque submarino Maricá, é cada vez mais necessária uma abordagem de detalhamento e integração de dados. Recomenda-se explorar mais a viabilidade e eficácia da Geomorfologia Sísmica em encurtar a lacuna de resolução entre o dado sísmico e o dado de poços/testemunhos.

Os dados de declividade dos canais e da sinuosidade foram bastante compatíveis com os dados observados em outros estudos, com a ressalva de que os canais de talude aparentam envolver outros processos sedimentares formados em contexto geográfico distinto. Ainda falta uma melhor compreensão de como a morfologia dos canais se altera em função das propriedades do fluxo, da declividade e da topografia do substrato.

REFERÊNCIAS

ANP – Agência Nacional de Petróleo, Gás Natural e Biocombustível, 2020. http://geo.anp.gov.br/mapview. Acesses: 26/10/2020.

Assine, M.L., Corrêa, F.S., Chang, H.K., 2008. Migração de depocentros na Bacia de Santos: importância na exploração de hidrocarbonetos. Revista Brasileira de Geociências. 38(2), 111–127.

Babonneau, N., Cattaneo, A., Savoye, B., Barjavel, G., Déverchère, J., Yelles, K., 2012. The Kramis deep-sea fan off western Algeria: Role of sediments waves in turbiditic levee growth, in: Prather, B.E., Deptuck, M.E., Mohrig, D., Van Hoorn, B., Wynn, R.B. (Eds.), Application of the Principles of Seismic Geomorphology to Continental-Slope and Base-of-Slope Systems: Case Studies from Seafloor and Near-Seafloor Analogues. Society of Exploration Geophysicists, pp. 293–308.

Babonneau, N., Savoye, B., Cremer, M., Klein, B., 2002. Morphology and architecture of the present canyon and channel system of the Zaire deep-sea fan. Marine and Petroleum Geology. 19, 445–467.

Bell, D., Kane, I.A., Pontén, A.S.M., Flint, S.S., Hodgson, D.M., Barrett, B.J., 2018. Spatial variability in depositional reservoir quality of deep-water channel-fill and lobe deposits. Marine and Petroleum Geology. 98, 97–115.

Bouma, A.H., 2001. Fine-grained submarine fans as possible recorders of long- and short-term climatic changes. Global and Planetary Changes. 28, 85–91.

Bouma, A.H., Coleman, J.M., Scientists, D.L. 96 S., 1985. Mississippi Fan: Leg 96 Program and Principal Results, in: Submarine Fans and Related Turbidite Systems. pp. 247–252.

Bowman, D., 2019. Principles of alluvial fan morphology. Springer.

Bryant, I., Herbst, N., Dailly, P., Dribus, J.R., Fainstein, R., Harvey, N., McCoss, A., Montaron, B., Quirk, D., Tapponnier, P., 2012. Basin to Basin: Plate Tectonics in Exploration. Oilfield Review - Autumn 2012. 4(3), 38–57.

Carlotto, M.A., Rodrigues, L.F., 2009. O Escorregamento Maricá - anatomia de um depósito de fluxo gravitacional de massa do Maastrichtiano, Bacia de Santos. Boletim de Geociências da Petrobras. 18(1), 51–67.

Carlson, P.R., Cowan, E.A., Powell, R.D., Cai, J., 1999. Growth of a post-Little Ice Age submarine fan, Glacier Bay, Alaska. Geo-Marine Letters. 19, 227–236.

Clift, P.D., 2017. Cenozoic sedimentary records of climate-tectonic coupling in the Western Himalaya. Progress in Earth and Planetary Science. 4(39), 1–22.

Contreras, J., Zühlke, R., Bowman, S., Bechstädt, T., 2010. Seismic stratigraphy and subsidence analysis of the southern Brazilian margin (Campos, Santos and Pelotas basins). Marine and Petroleum Geology. 27, 1952–1980.

Covault, J.A., 2011. Submarine fans and canyon-channel systems: A review of processes, products, and models. Nature Education Knowledge. 3(4).

Covault, J.A., Graham, S.A., 2010. Submarine fans at all sea-level stands: Tectono-morphologic and climatic controls on terrigenous sediment delivery to the deep sea. Geology. 28(10), 939–942.

Covault, J.A., Romans, B.W., 2009. Growth patterns of deep-sea fans revisited: Turbidite-system morphology in confined basins, examples from the California Borderland. Marine Geology. 265, 51–66.

Covault, J.A., Sylvester, Z., Hubbard, S.M., Jobe, Z.R., Sech, R.P., 2016. The stratigraphic record of submarine-channel evolution. The Sedimentary Record. 14(3), 4–11.

Covault, J.A., Sylvester, Z., Hudec, M.R., Ceyhan, C., Dunlap, D., 2019. Submarine channels “swept” downstream after bend cutoff in salt basins. Depositional Record. 00, 1–14.

Curray, J.R., Emmel, F.J., Moore, D.G., 2003. The Bengal Fan: morphology, geometry, stratigraphy, history and processes. Marine. 19, 1191–1223.

Delorme, P., Devauchelle, O., Barrier, L., Métivier, F., 2018. Growth and shape of a laboratory alluvial fan. Physical Review E. 98, 1–9.

Deptuck, M.E., Piper, D.J.W., Savoye, B., Gervais, A., 2008. Dimensions and architecture of late Pleistocene submarine lobes off the northern margin of East Corsica. Sedimentology. 55(4), 869–898.

Deptuck, M.E., Sylvester, Z., 2018. Submarine fans and their channels, levees, and lobes, in: Micallef, A., Krastel, S., Savini, A. (Eds.), Submarine Geomorphology. Springer, pp. 273–299.

Doughty-Jones, G., Mayall, M., Lonergan, L., 2017. Stratigraphy, facies, and evolution of deep-water lobe complexes within a salt-controlled intraslope minibasin. AAPG Bulletin. 101(11), 1879–1904.

Ercilla, G., Alonso, B., Baraza, J., Casas, D., Chiocci, F.L., Estrada, F., Farrán, M., Gonthier, E., Pérez-Belzuz, F., Pirmez, C., Reeder, M., Torres, J., Urgeles, R., 1998. New high-resolution acoustic data from the “braided system” of the Orinoco deep-sea fan. Marine Geology. 146, 243–250.

Ferry, J.N., Mulder, T., Parize, O., Raillard, S., 2005. Concept of equilibrium profile in deep-water turbidite systems: effects of local physiographic changes on the nature of sedimentary process and the geometries of deposits, in: Hodgson, D.M., Flint, S.S. (Eds.), Submarine Slope Systems: Processes and Products. Geological Society of London, pp. 181–193.

Fisher, W.L., Galloway, W.E., Steel, R.J., Olariu, C., Kerans, C., Mohrig, D., 2021. Deep-water depositional systems supplied by shelf-incising submarine canyons: Recognition and significance in the geologic record. Earth-Science Reviews.

Foreman, B.Z., Lai, S.Y.J., Komatsu, Y., Paola, C., 2015. Braiding of submarine channels controlled by aspect ratio similar to rivers. Nature Geoscience. 8, 700–704.

Gamberi, F., Rovere, M., Dykstra, M., Kane, I.A., Kneller, B.C., 2013. Integrating modern seafloor and outcrop data in the analysis of slope channel architecture and fill. Marine and Petroleum Geology. 41, 83–103.

Gamboa, D., Alves, T.M., Cartwright, J., 2012. A submarine channel confluence classification for topographically confined slopes. Marine and Petroleum Geology. 35, 176–189.

Gee, M.J.R., Gawthorpe, R.L., 2006. Submarine channels controlled by salt tectonics: Examples from 3D seismic data offshore Angola. Marine and Petroleum Geology. 23, 443–458.

Gee, M.J.R., Gawthorpe, R.L., Bakke, K., Friedmann, S.J., 2007. Seismic Geomorphology and evolution of submarine channels from the Angolan continental margin. Journal of Sedimentary Research. 77, 433–446.

Georgiopoulou, A., Cartwright, J.A., 2013. A critical test of the concept of submarine equilibrium profile. Marine and Petroleum Geology. 41, 35–47.

Hadler-Jacobsen, F., Johannessen, E.P., Ashton, N., Henriksen, S., Johnson, S.D., Kristensen, J.B., 2005. Submarine fan morphology and lithology distribution: a predictable function of sediment delivery, gross shelf-to-basin relief, slope gradient and basin topography, in: Doré, A.G., Vining, B.A. (Eds.), Petroleum Geology: North-West Europe and Global Perspectives - Proceedings of the 6th Petroleum Geology Conference. Geological Society of London, pp. 1121–1145.

Hamblin, W.K., Christiansen, E.H., 2003. Earth's dynamic systems, 10th ed. Pearson.

Hesse, R., Klaucke, I., Khodabakhsh, S., Piper, D.J.W., Ryan, W.B.F., 2001. Sandy submarine braid plains: Potential deep-water reservoirs. AAPG Bulletin. 85(8), 1499–1521.

Janocko, M., Nemec, W., Henriksen, S., Warchoł, M., 2013. The diversity of deep-water sinuous channel belts and slope valley-fill complexes. Marine and Petroleum Geology. 41, 7–34.

Jegou, I., Savoye, B., Pirmez, C., Droz, L., 2008. Channel-mouth lobe complex of the recent Amazon Fan: The missing piece. Marine Geology. 252, 62–77.

Jiang, S., Weimer, P., Henriksen, S., Hammon III, W., 2012. 3D seismic stratigraphy and evolution of Upper Pleistocene deepwater depositional systems, Alaminos Canyon, northwestern deep Gulf of Mexico, in: Prather, B.E., Deptuck, M.E., Mohrig, D., Van Hoorn, B., Wynn, R.B. (Eds.), Application of the Principles of Seismic Geomorphology to Continental-Slope and Base-of-Slope Systems: Case Studies from Seafloor and Near-Seafloor Analogues. Society of Sedimentary Geology, pp. 309–327.

Jobe, Z.R., Howes, N.C., Auchter, N.C., 2016. Comparing submarine and fluvial channel kinematics: Implications for stratigraphic architecture. Geology. 44(11), 931–934.

Jobe, Z.R., Sylvester, Z., Parker, A.O., Howes, N., Slowey, N., Pirmez, C., 2015. Rapid adjustment of submarine channel architecture to changes in sediment supply. Journal of Sedimentary Research. 85, 729–753.

Kolla, V., 2007. A review of sinuous channel avulsion patterns in some major deep-sea fans and factors controlling them. Marine and Petroleum Geology. 24, 450–469.

Kolla, V., Bandyopadhyay, A., Gupta, P., Mukherjee, B., Ramana, D.V., 2012. Morphology and internal structure of a recent Upper Benga Fan-Valley complex, in: Prather, B.E., Deptuck, M.E., Mohrig, D., Van Hoorn, B., Wynn, R.B. (Eds.), Application of the Principles of Seismic Geomorphology to Continental-Slope and Base-of-Slope Systems: Case Studies from Seafloor and Near-Seafloor Analogues. Society of Sedimentary Geology, pp. 347–369.

Kolla, V., Bourges, P., Urruty, J.M., Safa, P., 2001. Evolution of deep-water Tertiary sinuous channels offshore Angola (west Africa) and implications for reservoir architecture. AAPG Bulletin. 85(8), 1373–1405.

Kolla, V., Posamentier, H.W., Wood, L.J., 2007. Deep-water and fluvial sinuous channels - Characteristics, similarities and dissimilarities, and modes of formation. Marine and Petroleum Geology. 24, 388–405.

Lemay, M., Grimaud, J.-L., Cojan, I., Rivoirard, J., Ors, F., 2020. Geomorphic variability of submarine channelized systems along continental margins: Comparison with fluvial meandering channels. Marine and Petroleum Geology. 115, 1–17.

Limaye, A.B., Grimaud, J.L., Lai, S.Y.J., Foreman, B.Z., Komatsu, Y., Paola, C., 2018. Geometry and dynamics of braided channels and bars under experimental density currents. Sedimentology. 65, 1947–1972.

Maier, K.L., Fildani, A., Paull, C.K., McHargue, T.R., Graham, S.A., Caress, D.W., 2013. Deep-sea channel evolution and stratigraphic architecture from inception to abandonment from high-resolution Autonomous Underwater Vehicle surveys offshore central California. Sedimentology. 60, 935–960.

Mattos, N.H., Alves, T.M., Scully, A., 2019. Structural and depositional controls on Plio-Pleistocene submarine channel geometry (Taranaki Basin, New Zealand). Basin Research. 31, 136–154.

Mayall, M., Jones, E., Casey, M., 2006. Turbidite channel reservoirs-Key elements in facies prediction and effective development. Marine and Petroleum Geology. 23, 821–841.

McHargue, T., Pyrcz, M.J., Sullivan, M.D., Clark, J.D., Fildani, A., Romans, B.W., Covault, J.A., Levy, M., Posamentier, H.W., Drinkwater, N.J., 2011. Architecture of turbidite channel systems on the continental slope: Patterns and predictions. Marine and Petroleum Geology. 28, 728–743.

Mello, M.R., Azambuja Filho, N.C., Bender, A., Barbanti, S.M., Takaki, T., Fontes, C.A., Mohriak, W., 2013. New Deepwater Frontiers an Ocean Apart. GeoExPro. 10(2).

Modica, C.J., Brush, E.R., 2004. Postrift sequence stratigraphy, paleogeography, and fill history of the deep-water Santos Basin, offshore southeast Brazil. AAPG Bulletin. 88(7), 923–945.

Mohriak, W., Nemčok, M., Enciso, G., 2008. South Atlantic divergent margin evolution: rift-border uplift and salt tectonics in the basins of SE Brazil, in: Pankhust, R.J., Trouw, R.A.J., Brito Neves, B.B., De Wit, M.J. (Eds.), West Gondwana: Pre-Cenozoic Correlations Acrros the South Atlantic Region. Geological Society, London, Special Publication, pp. 365–398.

Moreira, J.L.P., Madeira, C.V., Gil, J.A., Machado, M.A.P., 2007. Bacia de Santos. Boletim de Geociências da Petrobras. 15(2), 531–549.

Mutti, E., Ricci Lucchi, F., 1978. Turbidites of the northern Apennines: introduction to facies analysis. International Geology Review. 20(2), 125–166.

Normark, W.R., 1978. Fan Valleys, Channels, and Depositional Lobes on Modern Submarine Fans: Characters for Recognition of Sandy Turbidite Environments. AAPG Bulletin. 62(6), 912–931.

Normark, W.R., 1970. Growth Patterns of Deep-Sea Fans. AAPG Bulletin. 54(11), 2170–2195.

Peakall, J., Sumner, E.J., 2015. Submarine channel flow processes and deposits: A process-product perspective. Geomorphology. 244, 95–120.

Pettingill, H.S., Weimer, P., 2002. Worldwide deepwater exploration and production: Past, present, and future. The Leading Edge. 371–376.

Picot, M., Droz, L., Marsset, T., Dennielou, B., Bez, M., 2016. Controls on turbidite sedimentation: Insights from a quantitative approach of submarine channel and lobe architecture (Late Quaternary Congo Fan). Marine and Petroleum Geology. 72, 423–446.

Pirmez, C., Beaubouef, R.T., Friedmann, S.J., Mohrig, D.C., 2000. Equilibrium profile and baselevel in submarine channels: examples from Late Pleistocene systems and implications for the architecture of deepwater reservoir, in: Weimer, P. (Ed.), Deep-Water Reservoirs of the World. Society of Sedimentary Geology, pp. 782–805.

Pirmez, C., Flood, R.D., 1995. Morphology and structure of Amazon Channel, in: Flood, R.D., Piper, D.J.W., Klaus, A. (Eds.), Proceedings of the Ocean Drilling Program, Initial Reports. pp. 23–45.

Posamentier, H.W., Davies, R.J., Cartwright, J.A., Wood, L., 2007. Seismic geomorphology - an overview, in: Davies, R.J., Posamentier, H.W., Wood, L., Cartwright, J.A. (Eds.), Seismic Geomorphology: Applications to Hydrocarbon Exploration and Production. Geological Society, London, Special Publications, pp. 1–14.

Prélat, A., Covault, J.A., Hodgson, D.M., Fildani, A., Flint, S.S., 2010. Intrinsic controls on the range of volumes, morphologies, and dimensions of submarine lobes. Sedimentary Geology. 232, 66–76.

Quirk, D.G., Schødt, N., Lassen, B., Ings, S.J., Hsu, D., Hirsch, K.K., Von Nicolai, C., 2012. Salt tectonics on passive margins: examples from Santos, Campos and Kwanza basins, in: Alsop, G.I., Archer, S.G., Hartley, A.J., Grant, N.T., Hodgkinson, R. (Eds.), Salt Tectonics, Sediments and Prospectivity. Geological Society of London, pp. 207–244. https://doi.org/10.1144/SP363.10

Reece, R.S., Gulick, S.P.S., Horton, B.K., Christeson, G.L., Worthington, L.L., 2011. Tectonic and climatic influence on the evolution of the Surveyor Fan and Channel system, Gulf of Alaska. Geosphere. 7(4), 830–844.

Reimchen, A.P., Hubbard, S.M., Stright, L., Romans, B.W., 2016. Using sea-floor morphometrics to constrain stratigraphic models of sinuous submarine channel systems. Marine and Petroleum Geology. 77, 92–115.

Shanmugam, G., 2016. Submarine fans: A critical retrospective (1950–2015). Journal of Palaeogeography. 5(2), 110–184.

Twichell, D.C., Schwab, W.C., Kenyon, N.H., Lee, H.J., 1996. Breaching the levee of a channel on the Mississippi Fan, in: Gardner, J.V., Field, M.E., Twichell, D.C. (Eds.), Geology of the United States: The View from GLORIA. Cambridge University Press, pp. 85–96.

Walker, R.G., 1992. Turbidites and submarine fans, in: Walker, R.G., James, N.P. (Eds.), Facies Models - Response to Sea Level Change. Geological Association of Canada, pp. 239–264.

Walker, R.G., 1978. Deep-Water Sandstone Facies and Ancient Submarine Fans: Models for Exploration for Stratigraphic Traps. AAPG Bulletin. 62(6), 932–966.

Weimer, P., Link, M.H., 1991. Global Petroleum Occurrences in Submarine Fans and Turbidite Systems, in: Weimer, P., Link, M.H. (Eds.), Seismic Facies and Sedimentary Processes of Submarine Fans and Turbidite Systems. Springer Science+Business Media, pp. 9–67.

Wood, L.J., Mize-Spansky, K.L., 2009. Quantitative seismic geomorphology of a Quaternary leveed-channel system, offshore eastern Trinidad and Tobago, northeastern South America. AAPG Bulletin. 93(1), 101–125.

Wynn, R.B., Cronin, B.T., Peakall, J., 2007. Sinuous deep-water channels: Genesis, geometry, and architecture. Marine and Petroleum Geology. 24, 341–387.

Wynn, R.B., Talling, P.J., Masson, D.G., Le Bas, T.P., Cronin, B.T., Stevenson, C.J., 2012. The influence of subtle gradient changes on deep-water gravity flows: a case study from the Maroccan turbidite system, in: Prather, B.E., Deptuck, M.E., Mohrig, D., Van Hoorn, B., Wynn, R.B. (Eds.), Application of the Principles of Seismic Geomorphology to Continental-Slope and Base-of-Slope Systems: Case Studies from Seafloor and Near-Seafloor Analogues. Society of Sedimentary Geology, pp. 371–383.

Zalán, P.V., Oliveira, J.A.B., 2005. Origem e evolução estrutural do Sistema de Rittes Cenozóicos do Sudeste do Brasil. Boletim de Geociencias da Petrobras. 13(2), 269–300.

Zhang, J., Wu, S., Hu, G., Fan, T. en, Yu, B., Lin, P., Jiang, S., 2018. Sea-level control on the submarine fan architecture in a deepwater sequence of the Niger Delta Basin. Marine and Petroleum Geology. 94, 179–197.

Zhang, J.J., Wu, S.H., Fan, T.E., Fan, H.J., Jiang, L., Chen, C., Wu, Q.Y., Lin, P., 2016. Research on the architecture of submarine-fan lobes in the Niger Delta Basin, offshore West Africa. Journal of Palaeogeography. 5(3), 185–204.

APÊNDICE 1

Figuras dos horizontes 1-5 em alta resolução e sem a identificação e classificação dos elementos deposicionais e morfológicos.

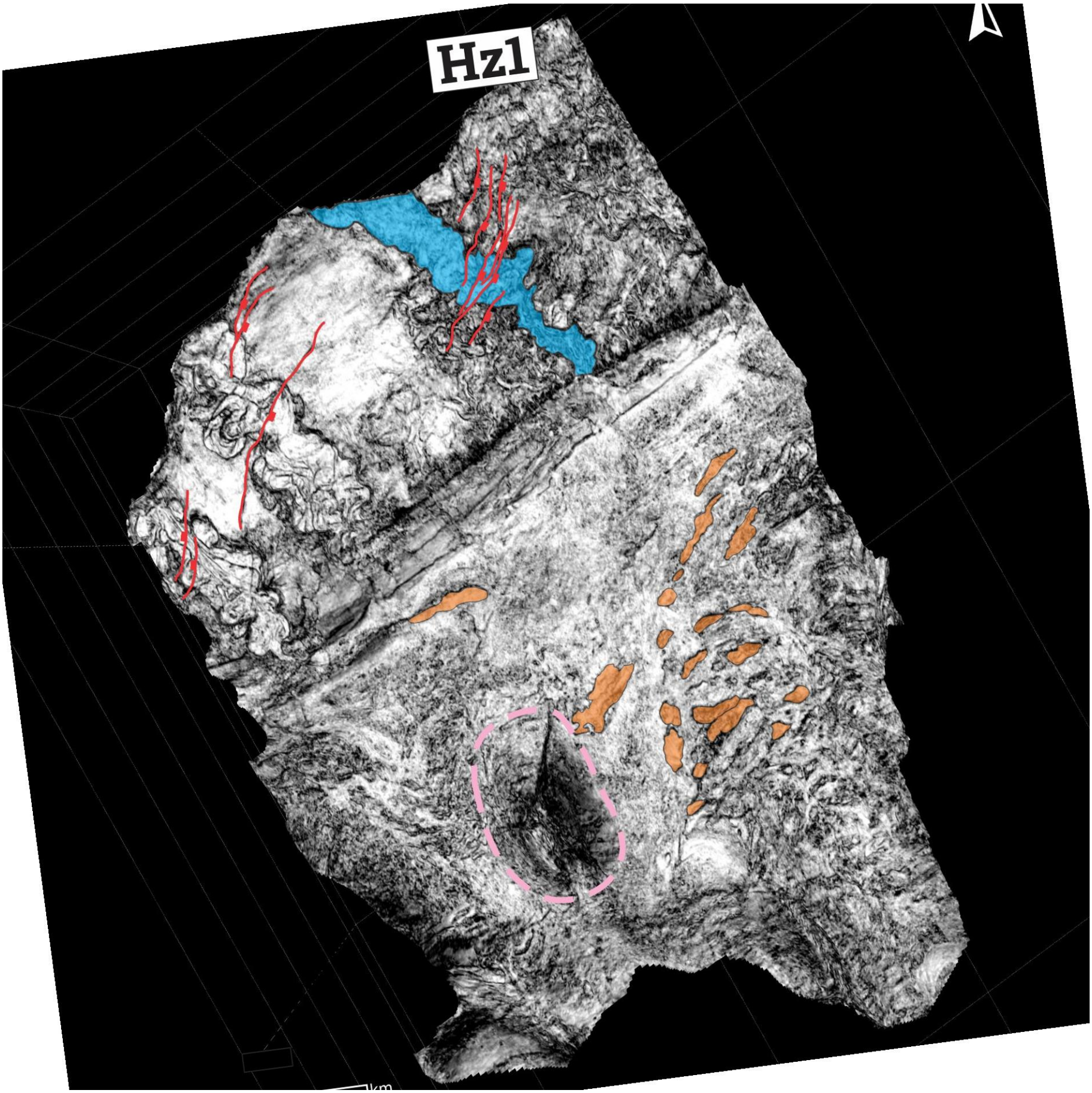

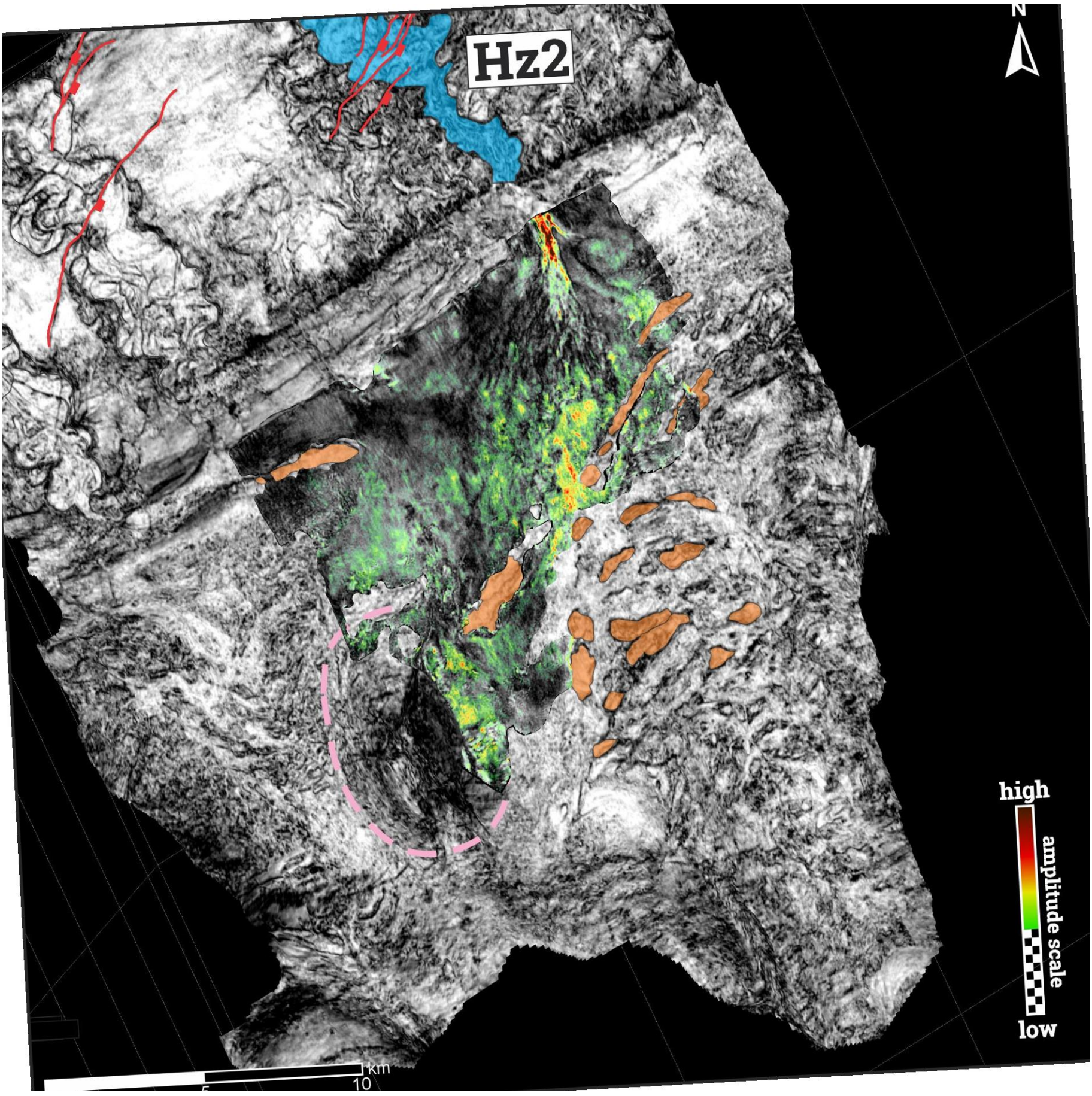
Hz2
N
high
amplitude scale
low
1km
10

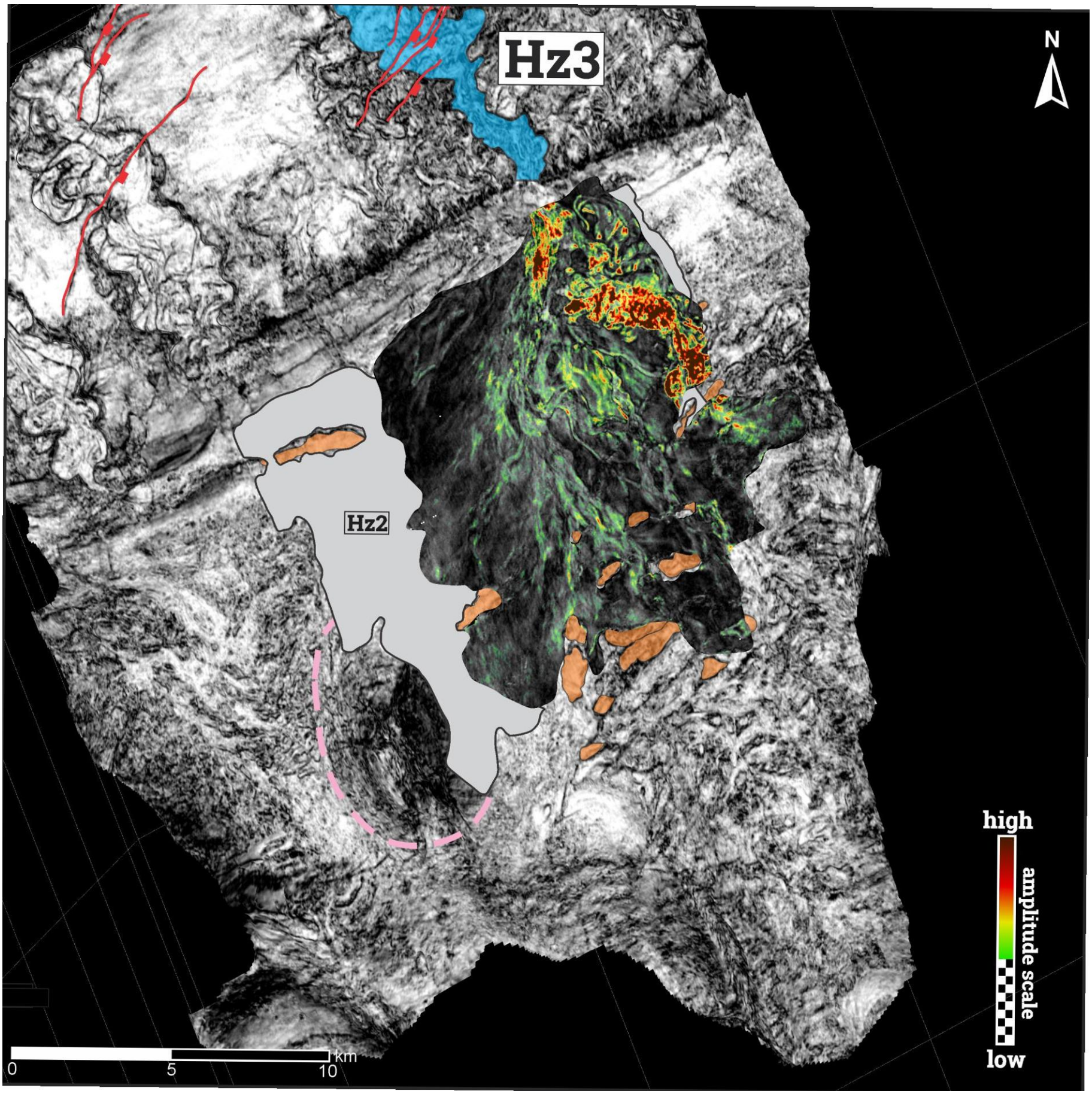
Hz3
Hz2
N
high
amplitude scale
low
0
5
10
km

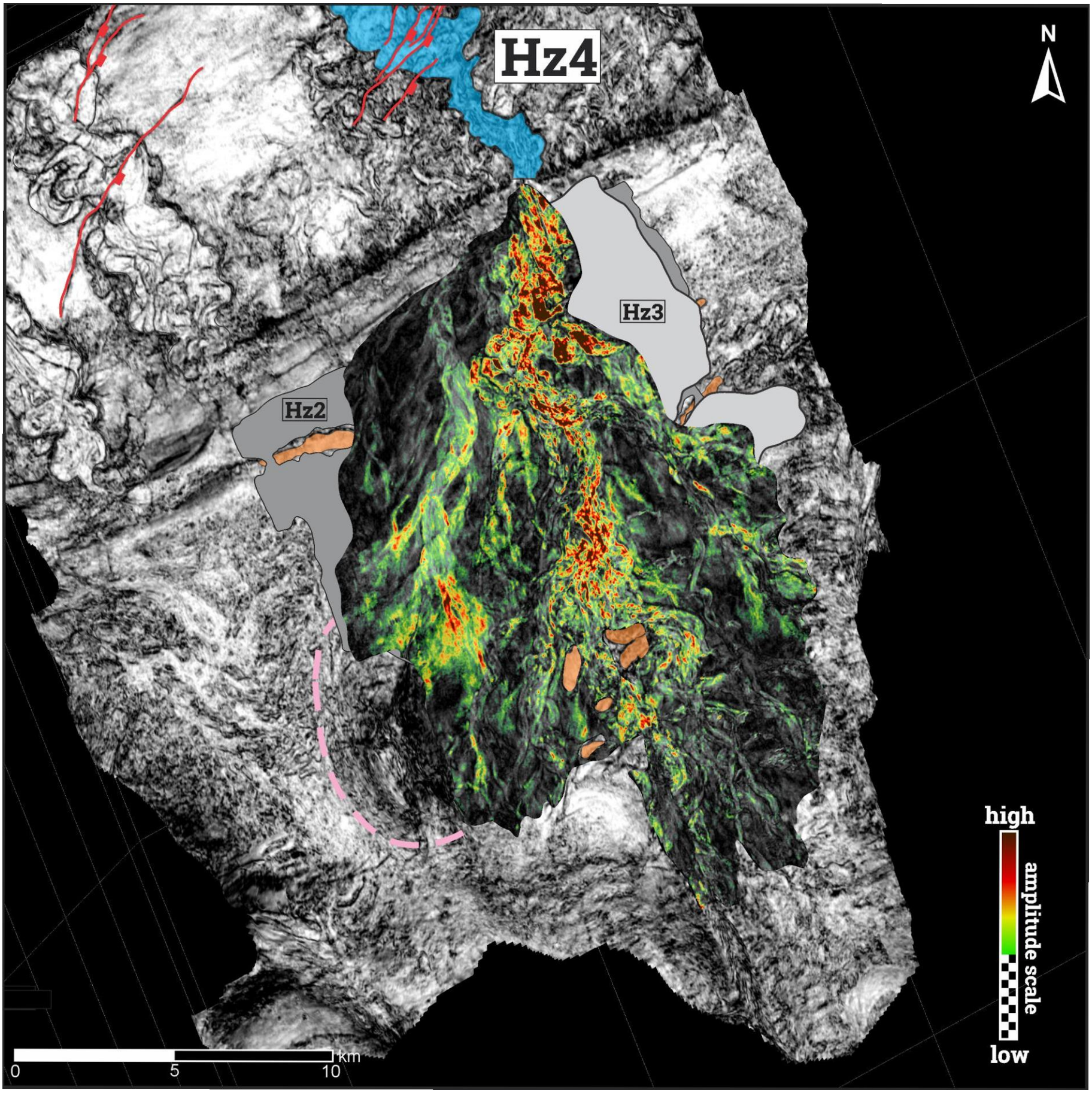
Hz4
Hz3
Hz2
N
high
amplitude scale
low
0
5
10
km

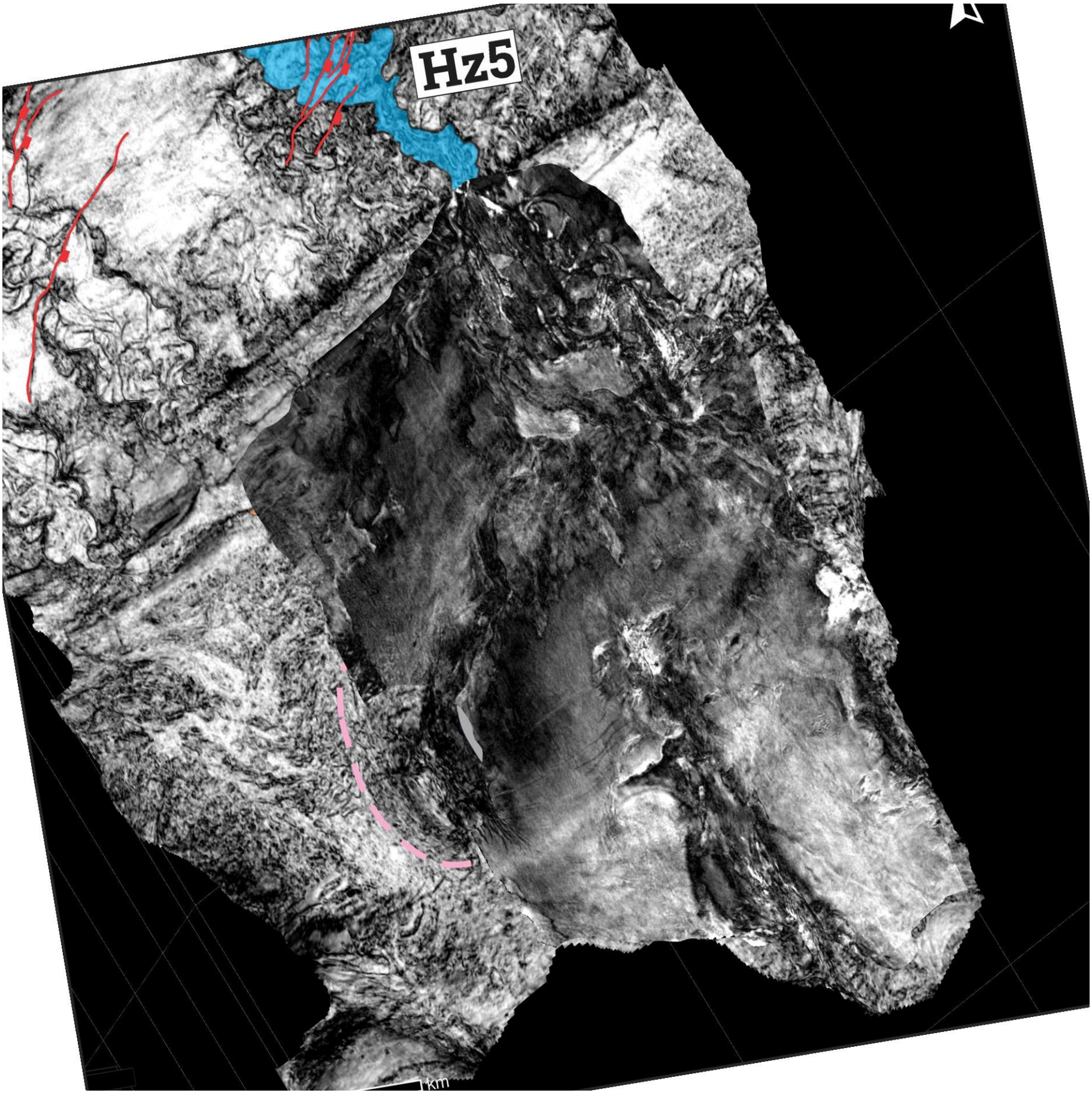
Hz5
1 km

APÊNDICE 2

Tabela de dados do comprimento, sinuosidade e declividade dos 113 canais.

Horizonte	Lobo	Distância do canal (m)	Distância dos extremos do canal (m)	Sinuosidade	ΔZ (m)	Declividade	Declividade (graus)	Declividade (%)
Hz2	L1	5659,76	5470,19	1,035	54,69	0,010	0,573	1,000
	L1	5531,89	5276,15	1,048	49,48	0,009	0,537	0,938
	L1	4586,59	4444,27	1,032	40,39	0,009	0,521	0,909
	L1	4385,51	4267,98	1,028	54,89	0,013	0,737	1,286
	L1	5280,37	5060,11	1,044	61,84	0,012	0,700	1,222
	L1	5583,42	5341,65	1,045	78,06	0,015	0,837	1,461
	L1	5117,36	4892,58	1,046	54,42	0,011	0,637	1,112
	L1	4766,00	4593,24	1,038	70,30	0,015	0,877	1,531
	L1	6141,94	5947,91	1,033	49,41	0,008	0,476	0,831
	L1	1725,83	1700,20	1,015	36,81	0,022	1,240	2,165
	L1	2078,29	1975,25	1,052	56,72	0,029	1,645	2,872
	L1	565,33	555,45	1,018	38,52	0,069	3,967	6,935
	L1	625,19	584,95	1,069	24,71	0,042	2,419	4,224
	L1	8555,68	7982,75	1,072	75,44	0,009	0,541	0,945
	L1	3738,37	3638,96	1,027	39,71	0,011	0,625	1,091
	L1	4010,65	3790,03	1,058	54,38	0,014	0,822	1,435
	L1	2664,76	2564,60	1,039	31,46	0,012	0,703	1,227
	L1	6195,89	5796,21	1,069	48,77	0,008	0,482	0,841
	L1	4871,69	4552,62	1,070	24,64	0,005	0,310	0,541
Hz3	L2	11250,50	4533,78	2,481	7,65	0,002	0,097	0,169
	L2	5257,41	2502,46	2,101	62,32	0,025	1,427	2,490
	L2	5554,78	4365,47	1,272	38,99	0,009	0,512	0,893
	L3	11379,50	10461,04	1,088	60,63	0,006	0,332	0,580
	L3	8859,50	8313,95	1,066	46,52	0,006	0,321	0,560
	L3	8827,86	7696,06	1,147	13,07	0,002	0,097	0,170
	L3	9957,60	9043,89	1,101	46,82	0,005	0,297	0,518
	L3	5803,10	5494,27	1,056	50,67	0,009	0,528	0,922
	L3	6063,19	5778,51	1,049	28,45	0,005	0,282	0,492
	L3	6019,87	5713,14	1,054	31,10	0,005	0,312	0,544
	L3	4214,60	4072,71	1,035	29,45	0,007	0,414	0,723
	L3	3621,18	3517,69	1,029	25,99	0,007	0,423	0,739
	L3	5374,08	5044,85	1,065	56,06	0,011	0,637	1,111
	L3	8885,96	6647,88	1,337	41,63	0,006	0,359	0,626
	L3	7541,24	6701,10	1,125	36,36	0,005	0,311	0,543
	L3	6238,30	5433,55	1,148	24,87	0,005	0,262	0,458
	L3	8831,60	7716,89	1,144	79,55	0,010	0,591	1,031
	L3	4738,57	4486,99	1,056	26,91	0,006	0,344	0,600
	L3	6092,26	5809,38	1,049	59,52	0,010	0,587	1,025

	L3	5243,00	4956,79	1,058	80,50	0,016	0,930	1,624
	L3	7377,83	6797,79	1,085	70,67	0,010	0,596	1,040
	L3	3696,57	3564,96	1,037	27,77	0,008	0,446	0,779
	L3	6034,44	5825,41	1,036	23,11	0,004	0,227	0,397
	L3	4293,04	3831,40	1,120	56,13	0,015	0,839	1,465
	L3	3313,41	3019,74	1,097	41,99	0,014	0,797	1,391
	L3	5403,23	5064,17	1,067	69,77	0,014	0,789	1,378
	L3	4807,98	4341,19	1,108	99,49	0,023	1,313	2,292
	L3	2242,99	2002,40	1,120	8,34	0,004	0,239	0,416
	L3	1981,52	1825,72	1,085	57,68	0,032	1,810	3,159
	L3	6233,82	4891,34	1,274	37,73	0,008	0,442	0,771
	L3	3961,72	3274,94	1,210	60,57	0,018	1,060	1,850
	L3	2216,54	2032,36	1,091	12,72	0,006	0,359	0,626
	L4	8751,88	8156,21	1,073	48,81	0,006	0,343	0,598
	L4	3502,03	3241,14	1,080	50,48	0,016	0,892	1,557
	L4	4577,92	4477,20	1,023	54,99	0,012	0,704	1,228
	L4	5597,75	5119,53	1,093	39,94	0,008	0,447	0,780
	L4	3982,64	3716,92	1,071	11,21	0,003	0,173	0,302
Hz4	L4	9059,83	8217,14	1,103	57,65	0,007	0,402	0,702
	L4	9601,25	8158,91	1,177	47,71	0,006	0,335	0,585
	L4	8972,31	8283,14	1,083	105,48	0,013	0,730	1,273
	L4	4586,88	4295,43	1,068	40,49	0,009	0,540	0,943
	L4	4039,50	3844,60	1,051	35,74	0,009	0,533	0,930
	L4	3415,43	3386,95	1,008	58,44	0,017	0,989	1,725
	L4	9016,36	8400,94	1,073	62,68	0,007	0,427	0,746
	L4	16399,24	14397,27	1,139	13,53	0,001	0,054	0,094
	L4	11291,93	10025,82	1,126	106,13	0,011	0,606	1,059
	L4	9671,36	8760,93	1,104	115,45	0,013	0,755	1,318
	L4	15721,78	13745,21	1,144	35,52	0,003	0,148	0,258
	L4	7696,51	6861,30	1,122	38,13	0,006	0,318	0,556
	L4	3736,79	3513,94	1,063	31,98	0,009	0,521	0,910
	L4	8429,68	7868,06	1,071	78,12	0,010	0,569	0,993
	L4	7661,20	6694,34	1,144	72,40	0,011	0,620	1,082
	L4	4264,64	4125,53	1,034	53,02	0,013	0,736	1,285
	L5	16756,29	14913,11	1,124	129,28	0,009	0,497	0,867
	L5	16061,72	14760,09	1,088	91,09	0,006	0,354	0,617
	L5	7903,69	7234,74	1,092	88,96	0,012	0,704	1,230
	L5	4443,54	4132,27	1,075	24,28	0,006	0,337	0,588
	L5	16132,58	14393,41	1,121	131,66	0,009	0,524	0,915
	L5	4382,38	3855,84	1,137	13,22	0,003	0,196	0,343
	L5	23370,59	20531,95	1,138	113,17	0,006	0,316	0,551
	L5	12291,48	11222,65	1,095	15,06	0,001	0,077	0,134
	L5	11983,77	11046,86	1,085	69,98	0,006	0,363	0,633
	L5	8325,75	7136,44	1,167	59,92	0,008	0,481	0,840
	L5	4902,33	4736,25	1,035	69,85	0,015	0,845	1,475

	L5	11250,75	10244,81	1,098	73,83	0,007	0,413	0,721
	L5	5344,23	4637,80	1,152	61,68	0,013	0,762	1,330
	L5	19007,43	15671,60	1,213	99,16	0,006	0,363	0,633
	L5	4570,91	4101,33	1,114	49,91	0,012	0,697	1,217
	L5	9624,97	8907,07	1,081	9,36	0,001	0,060	0,105
	L5	17503,93	14963,88	1,170	64,76	0,004	0,248	0,433
	L5	9640,08	8249,94	1,169	92,04	0,011	0,639	1,116
	L5	8422,43	6697,77	1,257	99,84	0,015	0,854	1,491
	L5	5717,31	5299,99	1,079	58,85	0,011	0,636	1,110
	L5	4412,85	3431,45	1,286	32,06	0,009	0,535	0,934
	L5	8914,60	7667,67	1,163	28,82	0,004	0,215	0,376
	L5	6438,62	6143,47	1,048	121,76	0,020	1,135	1,982
	L5	9009,12	7862,85	1,146	22,99	0,003	0,168	0,292
	L5	12823,28	11437,52	1,121	37,13	0,003	0,186	0,325
	L5	15860,57	14289,12	1,110	39,02	0,003	0,156	0,273
	L5	6869,65	5984,38	1,148	10,43	0,002	0,100	0,174
	L5	2258,31	2047,59	1,103	15,01	0,007	0,420	0,733
	L5	5303,34	5142,40	1,031	31,49	0,006	0,351	0,612
	L5	9024,92	7743,72	1,165	14,19	0,002	0,105	0,183
	L5	5723,13	4696,50	1,219	19,36	0,004	0,236	0,412
	L6	8987,72	7999,25	1,124	32,51	0,004	0,233	0,406
	L6	8186,23	7545,59	1,085	101,81	0,013	0,773	1,349
	L6	7579,27	6470,94	1,171	56,30	0,009	0,498	0,870
	L6	20648,46	4910,29	1,177	49,16	0,010	0,574	1,001
	L6	6178,71	5755,65	1,074	47,99	0,008	0,478	0,834
	L6	12382,54	11629,85	1,065	29,19	0,003	0,144	0,251
	L6	5777,60	5403,14	1,069	50,72	0,009	0,538	0,939
	L6	4351,96	3929,06	1,108	18,16	0,005	0,265	0,462
	L6	5188,89	4736,36	1,096	38,58	0,008	0,467	0,815
	L6	5771,44	5337,73	1,081	17,86	0,003	0,192	0,335